Fiber Optic Sensing with Lossy Mode Resonances: Applications and Perspectives

Fiber Optics Sensing With Lossy Mode Resonances: Applications and Perspectives

Francesco Chiavaioli, *Member, OSA, Member SPIE*, and Davide Janner

(Invited paper)

***Abstract*—This review focuses on the recent advances in lossy more resonance (LMR) fiber optics sensors. LMR sensors present many interesting feature also in comparison with surface plasmon resonance (SPR), the most widespread resonance-based sensing platform. Two key parameters determine LMR sensors performance: their geometrical configuration and the material supporting the lossy mode resonance. After reviewing those aspects and some fundamentals of the theory the review focuses on the sensing mechanisms, mainly based on refractometry, and their possible applications. Many examples from the literature are reported ranging from electric field to pressure sensors and from gas detection to bio-sensors. Such vibrant activity on LMR sensors confirms the potentiality of this technology making it a very promising platform for sensor development.**

***Index Terms*—Lossy mode resonances; surface waves; nanometer scale films; photonic platform; fiber optic applications; fiber sensing and biosensing**

I. Introduction

GUIDED-WAVE optics (GWO) encompasses the propagation and manipulation of light in thin-film dielectric waveguides and has allowed the study of novel physical phenomena over the years, representing an extraordinary tool for the development of innovative and reliable devices that provides fast, *in situ* or *in vivo*, real-time detection of physical parameters, chemical compounds or elements, and biomolecules[1]–[6]. Among GWO, fiber optic devices possess great advantages over other optical technology platforms given their peculiarities [7], [8]. In particular, they allow the exploitation of the fascinating and peculiar light management at unprecedented levels, which the other optical technologies can hardly attain [9]–[11].

The integration of fiber optics with micro/nano-technology has given the opportunity to develop highly sensitive, selective, repeatable and reproducible photonic devices, and even to underpin novel (bio-)sensing schemes for real applications [12]. Micro/nano-technology, like e.g. nanoparticles or nano films, allows tailoring the optical features of the device with outstanding spectral resolution, precision and accuracy, thus envisaging high performance optical platforms [13], [14].

Indeed, the interaction of light travelling within a fiber optic device and its surrounding enviroment can generate surface waves of different type, such as: evanescent, Bloch, surface plasmon polariton, lossy/leaky mode or derived from guided modes, etc. Those waves can be excited in many different ways [15] and are sensitive to every change occurring in the medium surrounding the fiber [16], [17] making them suitable for sensing applications.

Among surface wave sensors, surface plasmon resonance (SPR) is one of the most popular and widespread and employs metallic thin films to improve the performance of sensing/biosensing devices [18]. However, recently, starting from some studies on semiconductor waveguides [19], [20], the combination of metal-oxide or polymeric nanometric thin films with fiber optics has allowed to exploit lossy mode resonance (LMR) for sensing [21] rising a great interest in many field of applications. While both SPR and LMR exploits a thin material layer for supporting their relative modes, the generation mechanism of the lossy modes is related to the mode transition induced by a high refractive index thin film deposited onto a suitable substrate (e.g. optical fiber, coverslip, glass slide, etc.) [21]. For these different natures, SPR makes use of metal coatings (Au, Ag, etc.), whereas LMR of metal oxides or polymers. On the one hand, metals can't support LMR because of both the too low real refractive index (RI) and the too high losses. On the other hand, metal oxides present higher RI and low losses, especially in near-infrared region. Obviously, not all metal oxides can be used; in fact, the material extinction coefficient (losses) should not be neither 0 nor too large (<0.1). Fig. 1 depicts the comparison between SPR and LMR. It should be underlined that, differently from SPR, LMR have several interesting features that should not be underestimated: first, the excitationof both TE and TM light polarizations (SPR allows just TM polarization); second, the chance of tuning the LMR spectral wavelength by adjusting the film characteristics (very limited with SPR); third, the use of low-cost target materials as nanometric thin films (instead of metals); finally, the generation of more than one resonance with the same fiber optic device, which usually is not possible with SPR-based devices [22]. Aside these general rules for materials, a few metal oxides like

Francesco Chiavaioli acknowledges the National Research Council of Italy (CNR) for providing the financial support within the Short Term Mobility programs 2019 and 2017. Davide Janner acknowledges support from the interdepartmental laboratory CleanWaterCenter. The Authors acknowledge also the valuable discussions and insights with Prof. Ignacio Del Villar, Dr. Ambra Giannetti and Dr. Francesco Baldini in the preparation of this paper.

Francesco Chiavaioli is with the Institute of Applied Physics "Nello Carrara", National Research Council of Italy (CNR), 50019 Sesto Fiorentino, Firenze, Italy (e-mail: f.chiavaioli@ifac.cnr.it). Davide Janner is with Dipartimento di Scienza Applicata e Tecnologia (DISAT) and RU INSTM, Politecnico di Torino, Corso Duca degli Abruzzi 24, 10129 Torino, Italy (e-mail: davide.janner@polito.it).

indium tin oxide (ITO) can support both SPR and LMR in the

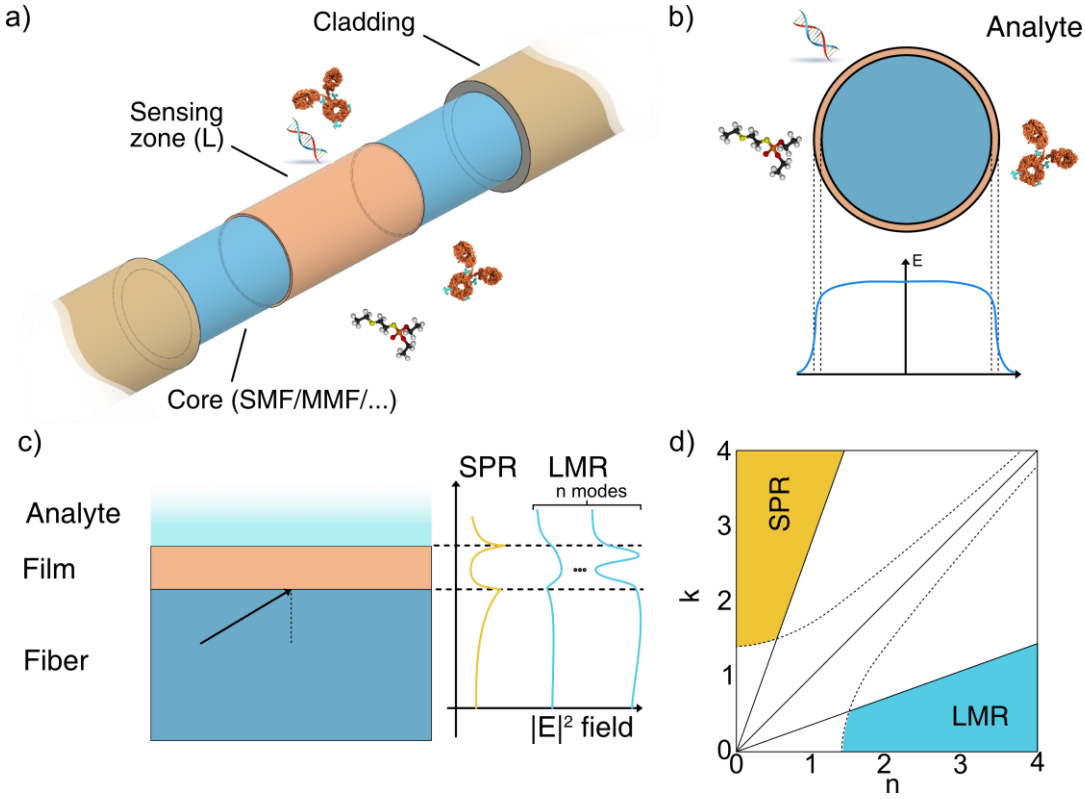

Fig. 1 Working principles of LMR. a) Sensing zone constituted by a thin film coating the fiber and interacting with b) the guided modes and the external environment (analyte). c) Comparison of SPR and LMR viewed in Kretschmann configuration as a thin film sensor. SPR sensors supports a single polarized mode that decays abruptly close to the interfaces while LMR sensors can support multiple LMR modes which have a significant part of the field in the film and tails in the analyte. d) Regions of the real (n) and imaginary (k) part of the refractive index that support SPR and LMR (after [22])

same device, making them ideal for combined sensing.[23]

This review is focused on LMR excited in fiber optics and is structured as follows. Section II provides some fundamentals on LMR including different fiber configurations (section IIA) and nanometric-scale materials (section IIB) that are key to effective generation of LMRs. Section III presents some LMR-based applications with fiber optics in physical (section IIIA), chemical (section IIIB) and biological (section IIIC) sensing. Finally, in Section IV we draw some conclusions and illustrate future perspectives in the field.

II. Lossy Mode Resonance: Fundamentals

In this section, we review the fundamentals of LMR fiber sensors by presenting a theoretical overview, the different configuration for the fiber and the main characteristics of materials that are used as thin film coating in LMR sensors.

A. *Theoretical overview*

The easiest theoretical approach to understand LMR in fibers comes from an extension of the mathematical treatment of SPR in Kretschmann configuration. This approach considers a ray of light incident to the surface of the sensing zone which can be constituted by a single or multi-layer thin film (see Fig. 2). The electromagnetic fields between two adjacent layers *n* and *n-1* are connected by the following equations [24]:

$$\begin{bmatrix} U_n \\ V_n \end{bmatrix} = M_{n-1} \begin{bmatrix} U_{n-1} \\ V_{n-1} \end{bmatrix}$$

Where the matrix M of the k-th layer can be written as:

$$M_k = \begin{bmatrix} M_{11} & M_{12} \\ M_{21} & M_{22} \end{bmatrix} = \begin{bmatrix} cos\ \beta_k & -j\frac{1}{q_k}\ sin\ \beta_k \\ -j\ q_k\ sin\ \beta_k & cos\ \beta_k \end{bmatrix}$$

With the following definitions

$$\beta_k = \frac{2\pi}{\lambda} n_k d_k \gamma$$

$$q_k^{TM} = \frac{Z_0}{n_k}\gamma$$

$$q_k^{TE} = \frac{n_k}{Z_0}\gamma$$

Being $Z_0 = \sqrt{\frac{\mu_0}{\epsilon_0}}$, $\gamma = \sqrt{1 - \left(\frac{n_1}{n_k}\right)^2 sin^2\,\theta}$, and θ the angle of incidence as indicated in Fig. 2. The *q* coefficients are different for TE and TM waves and are specified with superscripts.

If multiple layers are present, the matrix relating the incident fields coming from the fiber (n_1) and the field in the surrounding medium (n_N) is expressed as the product of the matrices of the single layers:

$$\begin{bmatrix} U_n \\ V_n \end{bmatrix} = \mathcal{M} \begin{bmatrix} U_1 \\ V_1 \end{bmatrix}$$

Where

$$\mathcal{M} = M_2\, M_3 \cdots M_{n-1} = \prod_{k=2}^{N-1} M_k$$

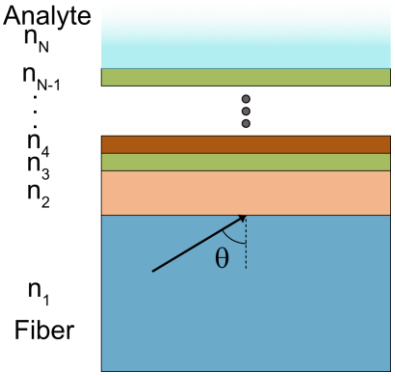

Fig. 2. Stack of a general N-layer fiber optics sensor.

$$\begin{bmatrix} U_n \\ \mathrm{V}_n \end{bmatrix} = \mathcal{M} \begin{bmatrix} U_1 \\ V_1 \end{bmatrix} \mathcal{M} = M_2\, M_3 \cdots M_{n-1} = \prod_{k=2}^{N-1} M_k \text{The}$$

$$\mathcal{M} = M_2\, M_3 \cdots M_{n-1} = \prod_{k=2}^{N-1} M_k \text{The}$$

$$r(\theta,\lambda) = \frac{(\mathcal{M}_{11} + \mathcal{M}_{12} q_N) q_1 - (\mathcal{M}_{21} + \mathcal{M}_{22} q_N)}{(\mathcal{M}_{11} + \mathcal{M}_{12} q_N) q_1 + (\mathcal{M}_{21} + \mathcal{M}_{22} q_N)} \quad (1)$$

Where using q^{TE} (q^{TM})we obtain the reflectivities r^{TE} (r^{TM}) for the TE (TM) modes. Equation (1) accounts for a single surface reflection, while in a fiber optics, more than one can take place at the interface of the fiber with the thin film in the sensing zone. Moreover, the ray description of light propagation in a fiber foresees that rays arrive at all the angles comprised between the critical angle θ_c which allows for total internal reflection and $\pi/2$ and θ_c is defined as:

$$\theta_c = \sin^{-1}\left(\frac{n_{cladding}}{n_{core}}\right) = \sin^{-1}\sqrt{1 - \left(\frac{NA}{n_{core}}\right)^2}$$

To account for these charactestics, the number of multiple reflections is obtained by simple geometrical considerations as:

$$N(\theta) = \frac{L}{D \tan\theta}$$

where, for the sake of clarity and without loss of generality, we neglected the contribution of the skewness since it can be readily included in the formulas following [25]. Considering the contribution of all the propagating rays and assuming a distribution of incident rays of the form *f(θ)* we can write the field reflectivity at λ as follows

$$R(\lambda) = \frac{1}{\int_{\theta_c}^{\frac{\pi}{2}} f(\theta) d\theta} \int_{\theta_c}^{\frac{\pi}{2}} f(\theta)[r(\theta,\lambda)]^{N(\theta)} d\theta$$

Where the first term integrates over the reys distribution and normalizes *R*, while *f(θ)* can take different functional forms as exemplified in the following:

$$f(\theta) = \begin{cases} k_0 n_{core} sin\theta cos\theta & [26] \\ exp\left[-\dfrac{\left(\theta - \frac{\pi}{2}\right)^2}{2W^2}\right] & [27] \\ \dfrac{n_{core}^2\, sin\theta\, cos\theta}{(1 - n_{core}^2\, cos^2\theta)^2} & [28] \end{cases}$$

If we consider unpolarized light for the interrogation of LMR, which is a typical case, the signal transmitted after the LMR sensor can be obtained as:

$$T(\lambda) = \frac{|R^{TE}(\lambda)|^2 + |R^{TM}(\lambda)|^2}{2} \quad (2)$$

From (2) we observe that the formalism used to deal with LMR and SPR starts differing. Indeed, SPR can support only TM modes while LMR can support both. However, apart from this last point the theoretical treatment is quite similar and so its their physical configuration, where a film on top of the fiber is responsible for the presence of LMR or SPR. In the simplest case of a single material film deposited on top of the fiber, the difference between these resonances lays in the film's refractive index characteristics and are summarized in table I.

TABLE I
LMR AND SPR CONDITIONS [ADAPTED FROM REF. [10]]

Resonance	Conditions for generation (n_{film}=n+j k)
Surface Plasmon Resonance (SPR)	$k>(\sqrt{2}+1)n$, $k^2-n^2>n^2_{core}$
Lossy Mode Resonance (LMR)	$k<(\sqrt{2}-1)n$, $k^2-n^2>n^2_{core}$

From Table I, it is clear that, while SPR can be generated with only a few materials that are tipically among the precious metals, LMR can be supported by a larger number of materials and in particular by metal oxides/polymers which present a good compatibility with the silica of the fiber optics and allows different options for their deposition on the fiber. For LMR excitation, the real part of permittivity must be positive and higher in magnitude than its own imaginary part and the real part of permittivity of waveguide material [10]. For these differences in the available materials for their excitation, SPRs are located in the visible region, while LMRs can be located in the visible or the near infrared region depending on the thickness of coating. The possibility of having near infrared resonances for LMR makes them very promising for fiber optics sensors.

Similarities between SPRs and LMRs extend to their dependence on the surrounding refractive index, thin film thickness, and refractive index similarly. However, we must underline that the dependence of the resonances behavior on the thickness is very different for SPR and LMR. Indeed, for sensing, SPR shows an optimal thickness of the coating layer that is mainly connected to the largest amount of field that is present in the surrounding medium [29]. SPR supports only one polarized mode and as the thickness grows above the optimal value, its sensitivity decays dramatically since more and more light is reflected and doesn't leak in the surrounding medium. In LMR, as the film thickness increases we observe a dramatic shift in the resonance wavelength up to the appearance of more than one LMR mode. Each LMR mode has its own sensitivity and that can be exploited to obtain a better characterization of the refractive index of the surrounding medium.

Another key difference between LMR and SPR is related to the typical excitation angles. In Kretschmann configuration, SPRs are obtained typically for angles in the range 40°-70° [16], whereas LMR typically are excited at near-grazing incidence (θ~90°) thus making them ideal to be used in fiber optics sensors.

Since LMR support both polarization, this leads to a spectrally broader resonance with respect to SPR thus reducing the resolution of measurements. To overcome this limitation, different approaches can be employed [48] among which the most conceptually simple is the excitation with controlled polarized light in combination with suitable configurations.

Since the theoretical framework is well consolidated, one can turn to consider the best configuration for sensing employing LMR. This task moves along two lines: fiber geometries and coating materials. Exploring and combining these two aspects, allows to push the sensing limits for fiber LMR sensors. For that, in the next subsections, we will focus on the different fiber configurations (section IIA) and on the nanometric-scale coating materials (section IIB) that are able to effectively generate LMRs.

B. Fiber Sensing Configurations

The literature accounts for several types of fiber sensing configurations that are used to generate LMRs and all the most relevant configurations are detailed in Fig. 3.

The firstly proposed apporach is named cladding-removed multimode fiber (CR-MMF). In this configuration, by chemically/mechanically removing the fiber jacket and cladding, the fiber core is directly exposed and thus, it can be directly coated with the LMR-supporting material (Fig. 3a).

Afterwards, other different fiber sensing configurations come out. By using singlemode fibers (SMFs), two distinct configurations have been proposed in order to permit the mode field to interact with the surrounding environment, and hence to be able excite LMRs: side-polished (or D-shaped) SMF and tapered SMF. The former (Fig. 3b) is surely not easy to fabricate with home-made systems but commercial options are available (Phoenix Photonics Ltd., UK). By customizing the side-polished length and depth (i.e. the distance from the fiber core to the fiber external border), it is possible to obtain highly sensitive devices by depositing a nanolayer onto the polished region. Typically, the polished length is around 10-20 mm, whereas the polished depth ranges in the order of a few microns (3-10 μm). In addition, it is worth pointing out that side-polished fibers maintain a good robustness and easy handling for real applications.

Tapered fibers represents another valuable option for implementing LMR-based devices. In that case, the coating material is deposited onto the tapered region of the fiber (Fig. 3c). Clearly, every sensing platform developed with tapered fibers suffers robustness issues in handling and might require further packaging complicating their usage.

Very recently, the use of microstructured fibers has been also proposed in the field of LMR-based device [30]. That option is surely fascinating, with room to open up several opportunities in different fields of sensing, though given its novelty it requires a deeper investigation with accurate and precise modeling and analysis.

For all possible configurations where the cylindrical geometry of the fiber is kept, a key element is the uniformity of the deposited material, aiming at the lowest possible roughness. According to the literature, the D-shaped SMFs exhibit the better performance for LMR in RI sensing and biosensing. This is coherent with the stronger light-matter interaction and the more uniform deposition of the LMR-generating material achievable onto the flat fiber surface.

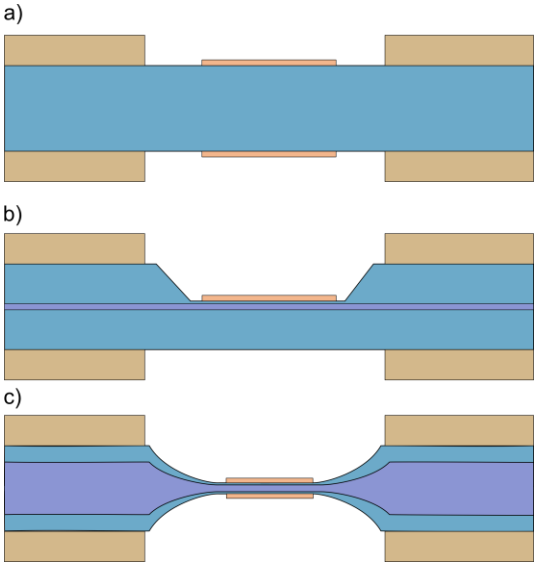

Fig. 3 Different configurations for LMR fiber sensors: (a) Cladding removed coated fiber, (b) D-shaped fiber obtained by side polishing and (c) tapered fiber

C. Thin-film Optical Features

The two major features that determine the optical characteristics of an LMR-based device are the thin film material permittivity ε and its thickness *d*.

The complex relative permittivity of each material can be expressed as [31]:

$$\varepsilon = \varepsilon' + j\varepsilon'' = \mathrm{Re}\{\varepsilon\} + j\,\mathrm{Im}\{\varepsilon\} = (n + jk)^2 \qquad (3)$$

where ε' describes the lossless permittivity, whereas ε" the lossy permittivity. In general, the first term represents the energy stored in the electric and magnetic fields, whereas the second term represents the energy lost as heat and dielectric leakage. In other words, ε' is the slowing down of light in a material, described by the RI, whereas ε" is the loss of energy or absorption of light, described by the absorption coefficient in the Lambert Beer law. Therefore, the previous equation can be rewritten in terms of *n* representing the material RI, and *k* describing the extinction coefficient that refers to how strongly a substance absorbs light at a given wavelength. These two parameters can be evaluated by spectroscopic methods. The gold standard is represented by ellipsometry, which is an optical technique for investigating the dielectric properties (complex refractive index or dielectric function) of thin films. This technique can be used to characterize several features, such as: composition, roughness, thickness (depth), crystalline nature, doping concentration, electrical conductivity, etc. Although very powerful as a tenchique, it is very complex and requires a

strong expertise to be employed combined with a delicate data processing to obtain the complex refractive index.

Different materials as high RI (HRI) dielectrics can be used in LMR. Indeed, many have been proposed[10], [32]–[34] such as: aluminum-doped zinc oxide (AZO), zinc oxide (ZnO), hafnium dioxide (HfO_2), zirconium dioxide (ZrO_2), tantalum oxide (Ta_xO_y), titanium dioxide (TiO_2), indium oxide (In_2O_3), indium gallium zinc oxide (IGZO), ITO, tin oxide (SnO_{2-x}), amorphous silicon, etc. Some HRI complex refractive indices (n,k) are shown in Fig. 4a and Fig. 4b and reported in Table II.

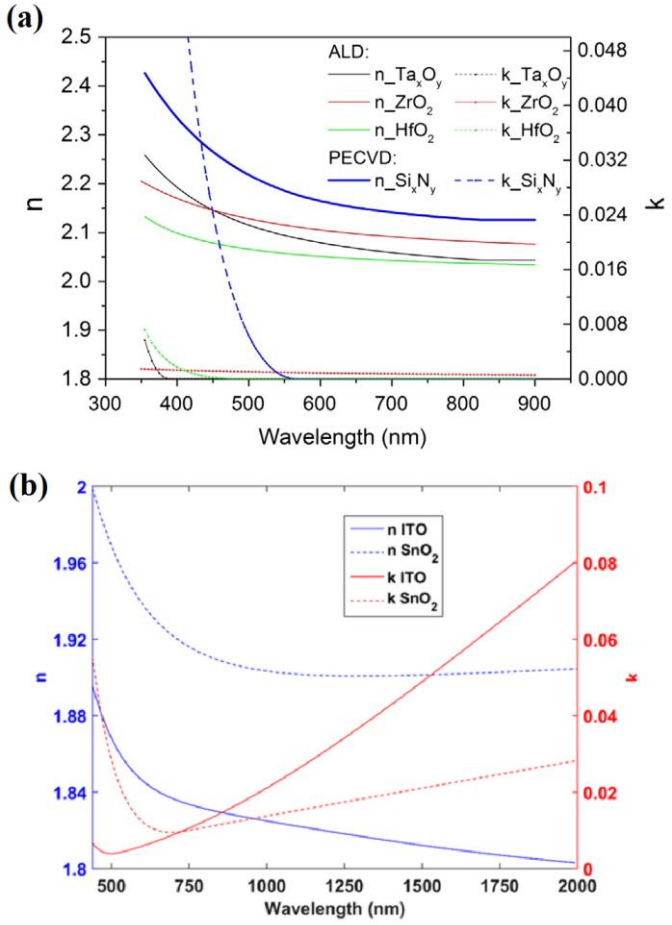

Fig. 4 (a) Dispersion characteristics in terms of n and k for HfO_2, ZrO_2, Ta_xO_y deposited by atomic layer deposition technique and for SixNy films deposited by plasma-enhanced CVD. [adapted from Ref. [32]. (b) Dispersion characteristics in terms of n and k for ITO and SnO_2 deposited by DC sputtering [adapted from Ref. [10]].

From a first glance, we can state that no single material allows attaining the best performance but it must be chosen depending on the applications to be developed also considering the operating wavelength of the device. It can be observed that n scales down with the wavelength (thus implying less LMR sensitivity according to the theory), but conversely the RI sensitivity increases at the same time. Therefore, a careful study and modeling of the device accounting for all the material features are mandatory. So far, SnO_2 seems to guarantee the greatest performance in terms of RI sensitivity of LMR-based devices for RI ranges close to a water environment.

The thickness of the thin film plays also a crucial role in optimizing the performance of an LMR-based device. There exists an optimized thickness for each thin film that allows generating an LMR that possesses the best optical features in terms of resonance bandwidth and visibility (or depth). This can be foreseen in advance by means of modeling and simulations. In addition, by controlling the polarization state of light (as said in the Introduction, both TM and TE polarizatons can be excited), the LMR resonance can be further improved. Typical values of thin film thickness range from tens of nm to hundreds of nm depending on the material. In general, a typical value is around 150 – 200 nm. Furthermore, another great option that LMR devices permit is the possibility of exciting more than one LMR, starting from the first LMR (always the most sensitive) up to the second, third, etc. [26]. The order of the LMR increases with the film thickness and, simultaneously, the LMR wavelength shifts towards longer wavelengths as well [35]. Finally, the deposition technique can also influence the device performance. Indeed, film adhesion, uniformity and roughness are critical parameters to pinpoint. In general, for LMR sensors we have the possibility of monitoring the deposition process in real time thus providing a great tool for the device optimization.

III. Lossy Mode Resonance: Applications

In this section, we present a state-of-the-art overview of the different where LMR-based devices and applications. The overview encompasses all the classical areas of sensing, such as physical, chemical and biological sensing.

A. Physical Sensing

The main physical parameter that can be measured by means of LMR-based devices is RI [32], [36]–[38] exploiting which many other physical quantities can be measured, e.g.: humidity [39], [40], voltage [41], electric current [42], pressure [30].

The measurement of RI using LMR-based devices is quite common in the literature since it is the sensing mechanism used to realize both optical refractometers underpinning volume or bulk RI changes and chemical sensors/biosensors underpinning surface or add-layer changes[43]. The performance of those devices in terms of RI sensitivity depends on two main aspects:

- optical features of coating material (both real and imaginary parts of material permittivity);
- evanescent field extension and amplitude.

Regarding the first point, it has been proved that the higher the real part of material permittivity (refractive index n), the better the RI sensitivity [34]. However, there are other effective parameters that should be considered. For instance, the imaginary part (extinction coefficient k) plays also a fundamental role since it determines the losses and has a strong influence on the resonance visibility (or depth) and its shape. It cannot be neither 0, nor too big (<0.1). Moreover, the target applications should also be considered. Indeed, in biosensing applications, some materials (i.e. ITO, SnO_{2-x}, HfO_2) present better robustness and biocompatibility, and reduced interference.

Regarding the second point the evanescent field extension and amplitude depend on the selected fiber mode, on the fiber geometry and on the optical features of the coating material. In particular, the mode related to the first LMR, so the first mode exhibiting a guided transition into the thin film, possesses the inherent highest RI sensitivity [30], [31], which is completely different from other fiber-based devices where the sensitivity improves with the increase in the mode order [10], [10], [10].

As far as the fiber geometry is concerned, optimized side-polished, tapered and microstructure fiber configurations permit to greatly improve the light-matter interaction of the fiber mode with the surrounding medium, and hence are preferable compared to unmodified or CR-MMFs [10].

TABLE II
OPTICAL FEATURES OF MOST OF THE INVESTIGATED LMR-GENERATING MATERIALS

Material	**Film thickness *d***	**Fiber configuration**	**RI range [RIU]**	**RI sensitivity [nm/RIU]**	**Reference**
zirconium dioxide (ZrO_2)	244 nm	CR-MMF	1.33 – 1.35	195	[32]
combined tantalum oxide and silicon nitride (Ta_xO_y/Si_xN_y)	560 nm (8.9% Ta_xO_y thickness percentages in the bilayer)	CR-MMF	1.33 – 1.35	1077	[32]
aluminum-doped zinc oxide (AZO)	167 nm	CR-MMF	1.3334 – 1.4471	1153.6	[44]
amorphous silicon	14 – 146 nm	D-shaped SMF	1.33 – 1.38	5300	[45]
zinc oxide (ZnO)	80 – 150 nm	D-shaped SMF	1.333 – 1.362	6700	[46]
indium oxide (In_2O_3)	25 – 180 nm	CR-MMF	1.32 – 1.37	4926	[47]
titanium dioxide (TiO_2) and poly(sodium 4-styrenesulfonate) PSS	126 nm	CR-MMF	1.3335 – 1.375	5268	[48]
titanium dioxide (TiO_2)	84 nm	D-shaped SMF	1.333 – 1.398	4122	[49]
indium gallium zinc oxide (IGZO)	426 nm	D-shaped SMF	1.37 – 1.385	6700	[50]
indium tin oxide (ITO)	170 nm	D-shaped SMF	1.365 – 1.38	7800	[51]
tin oxide (SnO_2) and SnO_2 nanoparticles	210 nm	CR-MMF	1.33 – 1.38	4704	[52]
tin oxide (SnO_{2-x})	160 nm	D-shaped SMF	1.321 – 1.326	14500	[34]
graphene oxide (GO)	102 nm	CR-MMF	1.39 – 1.42	12460	[53]

However, one should take into account a deterioration in sensor robustness and handling when modified geometry of the fiber is used, especially strong tapered fibers [54]. Therefore, the optimization of the performance can be attained by suitable choices but, in general, is a trade-off among the previous three points.

In order to attain the best RI sensing performance of LMR devices in terms of sensitivity, bandwidth and other comparative factors (i.e. *Q*-factor), according also to Table II, it seems that D-shaped fiber configuration coated with SnO_{2-x} or ZnO thin film could be the best option so far. In fact, this choice can guarantee a narrower bandwidth compared to CR-MMF and a higher sensitivity close to 1.33 RIU, so within the RI range of interest in biochemical applications. Obviously, nanotechnology and material science continue to go on and it is expected that new materials and novel fiber configurations will appear and will allow even better performances. Besides, it is worth pointing out that the factors and parameters here considered remain still valid for devices based on other surface guided waves like SPR and Bloch waves.

The use of metal-oxide nanoparticles is becoming a very promising alternative to excite high sensitive LMR. Very recently, TiO_2 nanoarray-based structures have been proposed to realize LMR-based fiber optics devices [55]. Two types of coating structures, TiO_2 nanoarrays without and with TiO_2 nanofilms (Fig. 5), are proposed, with a focus on the localized field distribution, the mode transmission characteristics and the sensitivity to surrounding RI changes. In the first structure, a localized electromagnetic field that can be generated by both TE and TM modes around nanoarrays is underpinned. By increasing the diameters of the nanoparticles and the fill factor (i.e. by decreasing the period or distance of nanoarrays), the LMR wavelength shifts towards longer wavelengths, thus improving the RI sensitivity [4], [43]. In the second structure, the localized electromagnetic field can be further improved due to the mode coupling between the nanofilms and nanoarrays. In this last case, a RI sensitivity of 5179 nm/RIU in the RI range

of 1.333–1.343 has been reported, with a 2-fold improvement compared to the structure without the TiO_2 nanoarrays.

Other physical parameters that can be measured with LMR-based sensors are of great interest towards the development of devices for real applications. The measurement of relative humidity (RH) stems from the changes induced by both the thickness and RI of a polymeric layer deposited around the

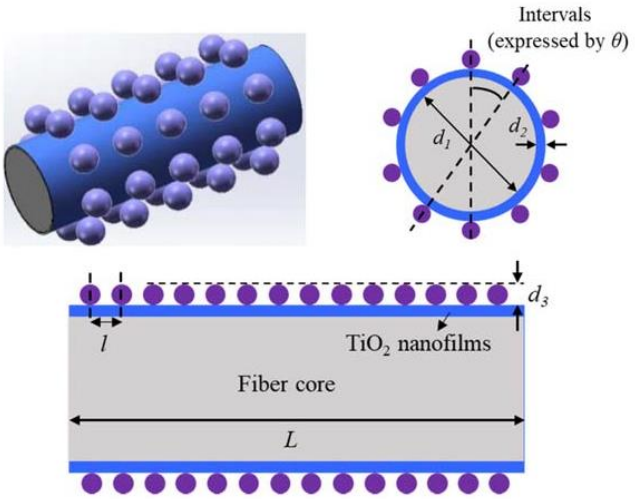

Fig. 5 TiO_2 nanofilms-nanoarrays deposited along a portion of the fiber core (3D mode, cross-section and longitudinal views). [adapted from Ref. [55]].

sensing region of the fiber. Polyallylamine hydrochloride (PAH) and polyacrylic acid (PAA) polymers[39], also in combination with Ag nanoparticles [40], are used as nano-films to implement relative humidity sensors. Fig. 6 shows the device realization, the experimental setup (Fig. 6a), and the response of the first LMR to RH changes when 20 bilayers of PAH/PAA (140 nm thickness) are used (Fig. 6b). The results confirm once more that the first LMR is the most sensitive resonance, even if the second LMR (not shown) can be made more sensitive with an optimized thickness of the nano-film.

Voltage [41] and electric current [42] are other two physical quantities that have been investigated with LMR-based devices for developing tunable electro-optic wavelength filters. For their measurement, a multilayer structure (Fig. 7a) is realized in order to underpin the excitation of LMR and to generate the shift of the LMR peak induced by an electro-optic material deposited between two electrodes. The first layer is used to generate the LMR and to work as the first electrode as well; the second layer allows tuning the optical features of the filter; finally, the outer layer represents the counter electrode. The first and last layers are made up of ITO, whereas the second layer consists of polyvinylidene difluoride (PVdF), a material which intrinsically possess a very large electro-optic effect induced by reversible molecular chain conformation change in relaxor ferroelectric terpolymers PVdF co-polymers [56]. Fig. 7b details the experimental setup for the proposed device, whereas Fig. 7c shows a SEM image of the cross section of the multilayer structure deposited onto the fiber and its magnified portion (Fig. 7d). The wavelength shift of the LMR permits to monitor electric field in current transformers in high voltage networks. Fig. 6e,f show the evolution of the transmission spectrum as a function of the applied voltage for the first LMR (Fig. 7e) and the second LMR (Fig. 7f).

In addition to the physical measurement presented, pressure variations can also be monitored with LMR-based devices [30]. In this case, a theoretical model and desing have been proposed by exciting LMR in microstructured fibers. The sensor is manufactured with an exposed-core photonics crystal fiber (PCF), on which a TiO_2/HfO_2/rubber polymer trilayer is

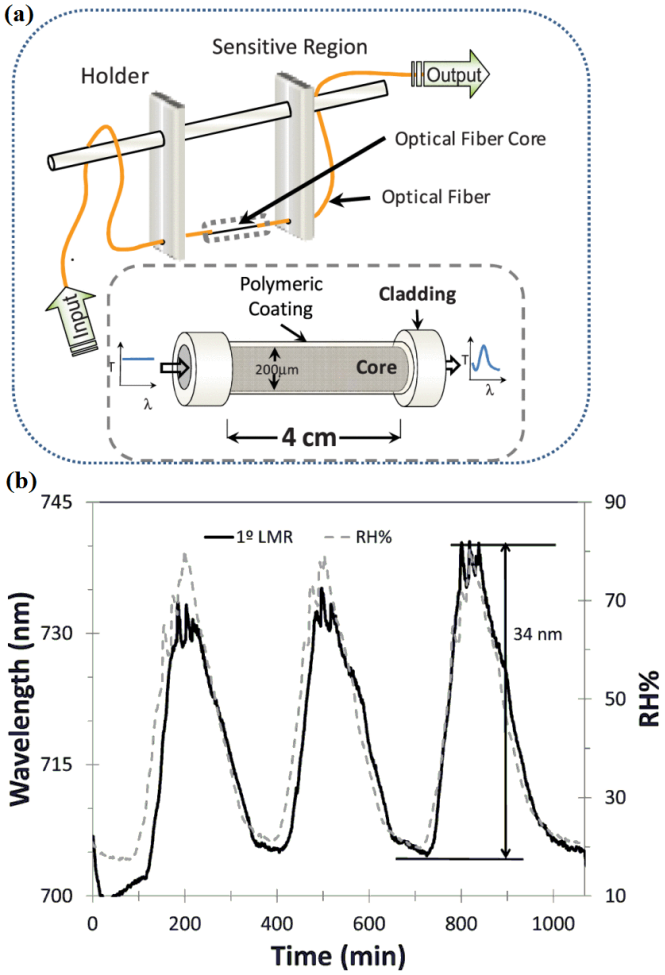

Fig. 6 (a) Details of the sensitive region. (b) Response of first LMR of [PAH/PAA]20 coated sensor to RH changes. [adapted from Ref. [39]].

deposited (Fig. 8a). Strong birefringence with x-polarized and y-polarized peaks is generated because of this asymmetry. Fig. 8b reports the electric field distributions and dispersion relations of core modes surrounded by a RI of 1.33, showing that the y-polarization has a higher coupling efficiency and the sensitivity of its peak is higher than that of the x-polarization. An extremely high RI sensitivity of 67 000 nm/RIU can be attained in the sensing range of 1.33–1.39, making it useful in chemical and bio-sensing applications in aqueous solutions.

The TiO_2/HfO_2 bilayer film dramatically increases the pressure sensitivity of the sensor reaching a peak of 5.0 μm/MPa. In addition, the performance of the sensor can be further optimized by adjusting the type and thickness of the film.

B. Chemical Sensing

Chemical compounds or elements can be effectively detected by LMR sensors. The most interesting examples include the detection of gases, such as hydrogen (H_2) [57] and hydrogen

sulfide (H_2S) [58], of volatile organic compounds (VOCs), such as ethanol [53], methanol and isopropanol [59], of ammonia in water [60], of pH [27] and of hydrogen peroxide (H_2O_2)[61]. Hydrogen detection, or hazardous gases in general, finds widespread applications in environmental monitoring for health and safety concerns

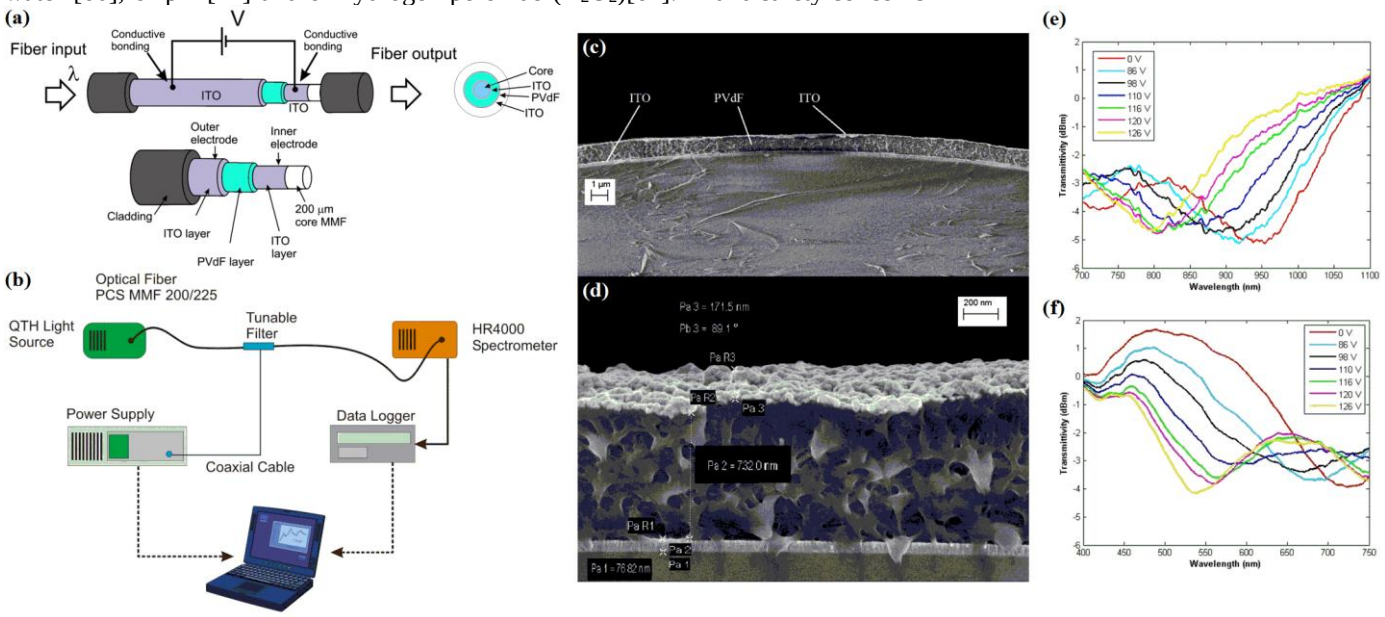

Fig. 7(a) Details of the fiber optics sensor and the multilayer structure deposited onto the fiber. (b) Experimental setup used to measure the voltage changes. (c) SEM image of the cross section of the multilayer structure and (d) of the magnified portion. Response of (e) first and (f) second LMRs for different voltages applied. [adapted from Ref. [41]].

Thanks to reversible interaction of metal oxides with gases, an LMR-based CR-MMFs coated with ITO nanofilm (about 20 nm thickness) and nanoparticles have been employed for the detection of H_2 [57]. a shows a SEM image of ITO nanoparticles, with an average spherical size of 60–80 nm. A wavelength shift of the peak absorbance towards longer wavelengths is observed as a function of the H_2 concentration. Three different sensing configurations are developed, where the coating layer consists of ITO thin film, ITO nanoparticles or ITO thin film + nanoparticles, and the comparison of the achieved results is detailed in b. It can be observed that the best performance refers to the use of the combination of ITO thin film and nanoparticles. Moreover, the proposed sensor is studied in terms of its selectivity towards common interfering gases (c), showing very promising results for its employment in real applications.

Another gas that has been investigated with LMR-based fiber devices is H_2S [58]. In this case, the LMR technique has been compared with SPR. Three types of sensors, two underpinning LMR and one employing SPR, are fabricated using CR-MMFs coated with ZnO in three different structures: combined thin film and nanoparticles, only nanoparticles (SEM image in Fig. 9a) and combined thin films of Ag and ZnO. The sensing principle is based on the measurement of wavelength shift of the peak absorbance as a function of the H_2S concentration (see the inset of Fig. 9b). The results detailed in Fig. 9b show that the best response to H_2S gas has been obtained with the first ZnO structure. In addition, the best sensor reveals good selectivity towards common interfering gases (Fig. 9c) thus to be used in real applications. Due to increasing pollutions all over the world, the requirements related to VOCs emissions are getting more stringent by the governmental legislations, and hence new technological solutions are necessary to monitor environmental changes. The use of LMR-based fiber optics devices has been proposed in the literature to detect some VOCs. One of the most interesting example employs an organometallic coating $[Au_2Ag_2(C_6F_5)_4(NH_3)_2]_n$ given its optical features that present reversible changes in presence of organic vapors [59]. Layer-by-layer (LbL) technique is employed to deposit the sensing material onto CR-MMF for a length of 2 cm. The final sensing layer, with several cycles using PAH and PAA solutions, consists of a tetralayer of [PAH/PAA/Suspension/PAA]. The repeated deposition of tetralayers underpins the generation of several LMRs, starting from the first with 11-17 tetralayers. Fig. 10a represents the theoretical realization of the proposed device where the LMRs are studied as a function of the number

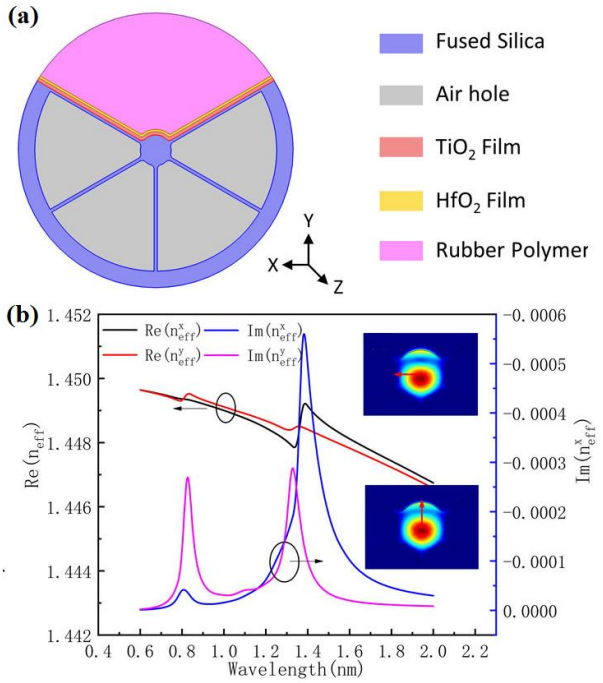

Fig. 8 (a) Details of the fiber optics sensor and the multilayer structure realized onto the fiber. (b) Electric field distributions and dispersion relations of core modes when the surrounding RI is 1.33. Insets: x -polarized core mode at λ = 808 nm (top) and y-polarized core mode at λ = 827 nm (bottom). [adapted from Ref. [30]]

of tetralayers deposited onto the fiber. Fig. 10b details a SEM image of the cross-section of the fiber coated with 28 tetralayers (roughly 1.107 μm). The sensor response stems from the adsorption process of the VOCs into the sensing matrix and from the reaction mechanism with the sensing material. Both processes depend basically on the VOC molecular size and the hydrophobicity. For these reasons, methanol, ethanol and isopropanol have been used because of their characteristics. Differently from the other examples, a spectral shift of the LMR towards shorter wavelengths is observed when the VOC concentration increases. This is just a consequence of the changes in the coating material when VOCs are present. Fig. 10c accounts for the spectral evolution of the second LMR located at around 780 nm when methanol at increasing concentrations is purged inside the measuring chamber. A linear relation between the LMR spectral shift and the methanol concentration in vapor from 0 to 250 ppm (v/v) can be extrapolated with a sensitivity of 0.131 nm ppm^{-1}. A similar linear trend is showed for the other two VOCs, with less sensitivity.

Graphene oxide (GO) together with SnO_2 have been also used for the implementation of an LMR-based fiber optics device to detect another VOC, i.e. ethanol [53]. A portion of CR-MMF is firstly coated with a thin film of SnO_2 and then a further coating made of 1, 2 and 4 bilayers of polyethyleneimine (PEI) and GO is deposited by LbL onto three fiber devices.

The experimental setup and the sketch of the sensing configurations are depicted in Fig. 12a. Fig. 12b details an homogeneous and uniform surface of 1-bilayer PEI/GO coating (SEM), whereas Fig. 12c shows the characteristic folds of GO nanosheets (AFM). The sensing behavior has been characterized and referenced with the sensor without GO by introducing in-water ethanol solutions at concentrations of 0%, 20%, 40%, 60%, 80% and 100% v/v. The sensors with GO report much better performance with a maximum sensitivity improvement of 176% with respect to the sensor without GO.

Ammonia is regarded as a highly hazardous chemical compound, and hence requires effective and reliable monitoring procedures. LMR phenomenon has been explored to detect ammonia by depositing a nanofilm of TiO_2, containing porphyrin as functional material (5,10,15,20-tetrakis(1-methyl-4-pyridinio)porphyrin tetra(p-toluenesulfonate); TMPyP), onto an adiabatic and non-adiabatic tapered fibers [60]. Adiabatic and non-adiabatic tapers of 17 μm and 40 μm waist diameters and of 4.5 mm long are fabricated in a boron-germanium co-doped fiber. The TiO_2 coating, deposited by the liquid phase deposition (LPD) technique, allows to generate an LMR in the transmission spectrum. Unmodified TiO_2 and combined TMPyP/TiO_2 nanocoatings are tested. In the first case, the non-uniform nanofilm is not able to generate LMR.

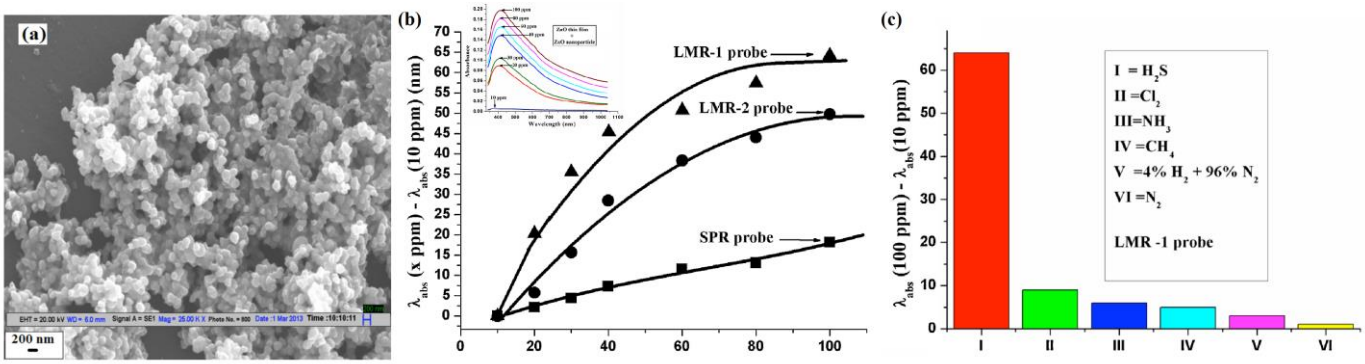

Fig. 9 (a) SEM image of ZnO nanoparticles. (b) Relative variation of the peak absorbance normalized to the value at 10 ppm as a function of concentration of the H_2 gas for the three fiber sensors coated with Ag and ZnO thin films (squares), ZnO nanoparticles (circles) and ZnO thin film + nanoparticles (triangles). The inset accounts for the sensing principle based on the measurement of wavelength shift of the peak absorbance as a function of the H_2S concentration. (c) Selectivity test for different gases, considering the LMR-based fiber sensor coated with ZnO thin film + nanoparticles. [adapted from Ref. [58]].

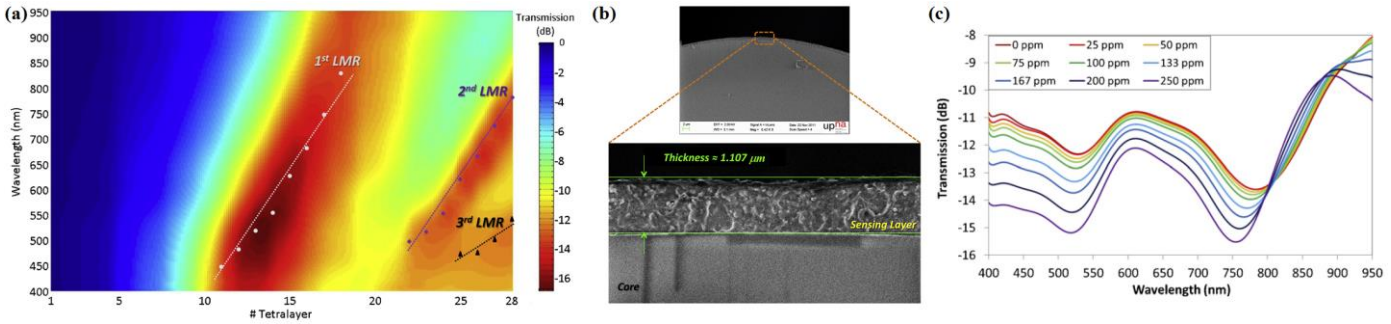

Fig. 10(a) Theoretical representation of the LMRs generated during the deposition of tetralayers. The experimental transmission minima of each LMR are indicated with white, blue and black symbols for the first, second and third LMR, respectively. (b) SEM image of the $[PAH/PAA/Suspension/PAA]_{28}$ coating deposited onto the fiber. (c) Transmission spectra of the second LMR as a function of different methanol concentrations. [adapted from Ref. [59]].

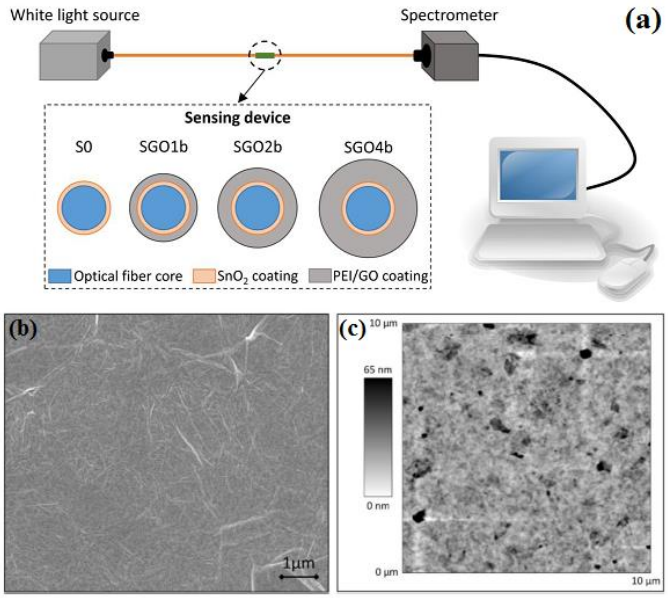

Fig. 11 (a) Fiber optics experimental setup and schematic structure of the three types of sensors. (b) SEM and (c) AFM images of the superficial structure of a 1-bilayer PEI/GO coating deposited onto a glass slide. [adapted from Ref. [53]].

The quality of the film is importantly improved, when the functional material is dissolved in the solution and it supports the realization of a highly uniform film. The 17 µm-diameter adiabatic taper has been finally selected to be the most suitable for LMR generation. The interaction of the porphyrin with ammonia induces a change in the RI of the coating, which in turn causes a change in the central wavelength of the LMR, thus allowing the measurement of concentrations of in-water ammonia as low as 0.1 ppm, with a response time of less than 30 s. Porphyrin has been chosen given its high selectivity towards target compounds and because it presents low cross-sensitivity to non-amine compounds, such as alcohols and carboxylic acids [60]. However, when the device is exposed with other amine compounds, a similar phenomenon can be foreseen, thus reducing the overall device selectivity. Fig. 12 accounts for the calibration curve when the sensor is exposed to ammonia at various concentrations from 0.1 ppm up to the saturation point of the sensor (10000 ppm). A detection limit of 0.16 ppm is attained.

The measurement of pH is of a huge interest in several fields, such as environmental, chemical and medical sciences. The use of the previously-mentioned PAH/PAA polymeric coating [39], [40], [59] has beed also proposed as pH sensitive nanofilm [27]. The behavior of this coating material that presents a change in the thickness as a function of pH of the surrounding solution not only permits the realization of fiber-based pH sensors based on the wavelength detection approach, but also allows a high degree of tunability in the excitation of LMRs. The sensing mechanism is based on the capability of swelling/deswelling of the PAH/PAA polymeric coating. As previously-discussed, several LMRs (from the first to the third) can be excited depending on the number of PAH/PAA bilayers deposited onto the sensing portion of the fiber.

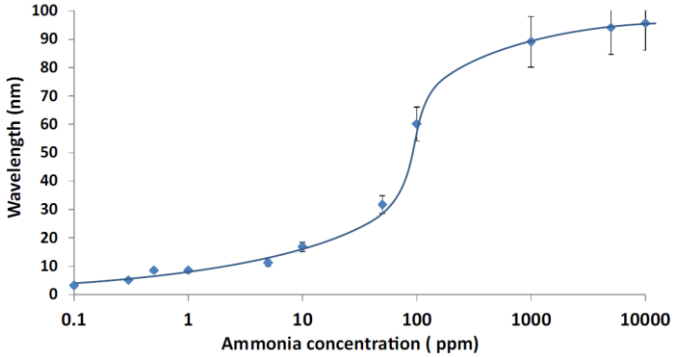

Fig. 12 Shift of LMR central wavelength as a function of ammonia concentrations (calibration curve) from 0.1 ppm to 10000 ppm. [adapted from Ref. [60]].

In order to compare the sensitivity of first and second LMRs in the detection of pH, two different devices are fabricated: the former consists of 100 bilayers $[PAH/PAA]_{100}$ exciting the second LMR, whereas the latter consists of 25 bilayers $[PAH/PAA]_{25}$ exciting the first LMR. Fig. 13a details a SEM image of the $[PAH/PAA]_{100}$ coating deposited onto the fiber with an average thickness of about 1.2 µm. Therefore, in case of the second device with $[PAH/PAA]_{25}$, the average thickness is expected to be around 300 nm. The results of this LMR-based fiber optics pH sensor are showed in Fig. 13b and c. The former figure details the spectral response in terms of changes in both the LMR wavelength and intensity for the device exciting the first LMR, when the sensitive region is alternatively immersed into pH 6 and pH 3 solutions at different time intervals. A wavelength shift of roughly 110 nm is observed. The latter figure accounts for the respective calibration curve within the investigated pH range (3 pH – 6 pH). Overall, an accuracy of ±0.001 pH units and an average sensitivity of 0.027 pH units/nm within the range between pH 3 and pH 6 are attained after an adequate design.

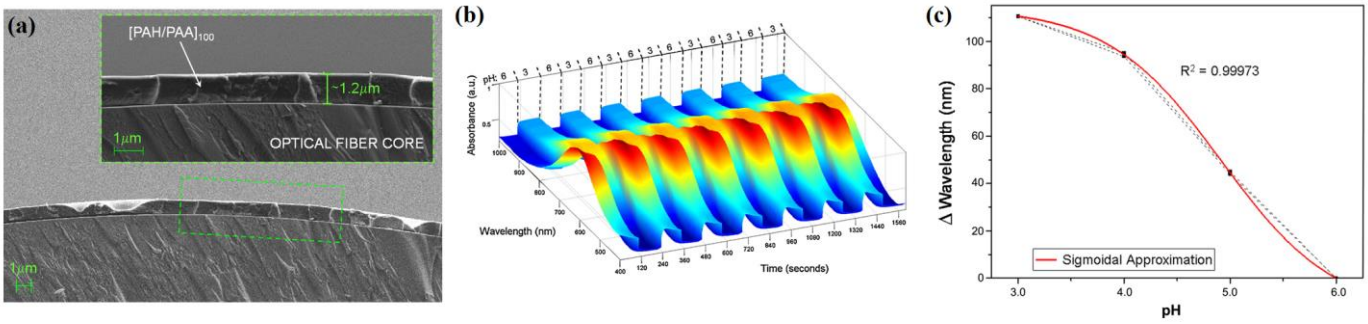

Fig. 13 (a) SEM image of the $[PAH/PAA]_{100}$ coating deposited onto the core of a CR-MMF. (b) Spectral response in terms of changes in both the LMR wavelength and intensity for the device exciting the first LMR, when the sensitive region is alternatively immersed into pH 6 and pH 3 solutions at different time intervals. (c) Calibration curve of the device exciting the first LMR within the range of 3 pH – 6 pH. [adapted from Ref. [27]].

One of the most interesting examples of LMR-based devices for chemical sensing reports the detection of H_2O_2, a very small molecule (34 g/mol molecular weight), in a very broad range from real samples of daily in-taking polyphenol rich beverages, such as green tea, black tea and coffee in a pseudo-corporal condition [61]. The fiber optic device is fabricated in two steps using the best combination of Ag nanoparticles and ZnO nanowedge (NWD) (Fig. 14a). A SEM image of the finalized nanostructure grown onto the fiber is shown in Fig. 14b with the optimized parameters. The thickness of the ZnO layer pinpoints the number of modes supported by the film. When the coupling of the evanescent wave with the mode supported by the nanostructure is satisfied, the maximum energy transfer occurs for a particular wavelength which is called in literature as peak absorbance wavelength (PAW) in the transmission spectrum. The combined structure underpins lossy modes in the absorbing ZnO thin film/nanostructure, whereas the resonance is excited between the evanescent wave generated due to the total internal reflection at the fiber–ZnO thin film boundary and the lossy modes of ZnO. The device works in two H_2O_2 concentration range; the first for *in vivo* applications covering the range that includes adequate, enduring and toxic levels in human body (< 300 μM) and the second for the range of H_2O_2 liberated by polyphenolic-daily consuming beverages (300 μM – 1500 μM). Fig. 14c and d account for the LMR absorbance spectra and measured PAWs for different concentrations of H_2O_2 solution in the two investigated regimes, respectively. The device shows a LOD of 82 nM, with a response time of roughly 30 s and good repeatability and reusability.

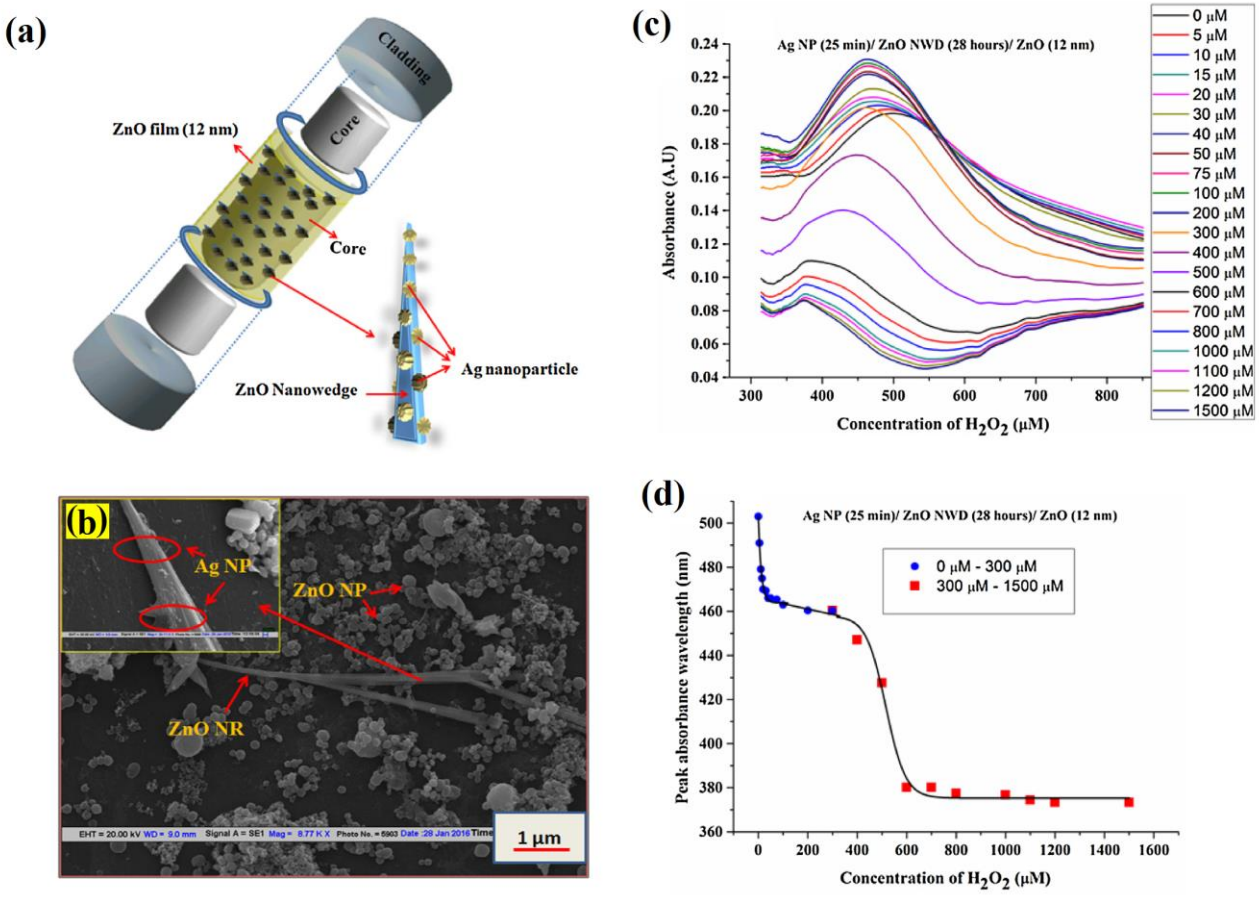

Fig. 14(a) Sketch of the sensing device with the realized nanostructure consisting of Ag NP/ZnO NWD/ZnO thin film. (b) SEM image of the finalized device (Ag NP (25 min)/ZnO NWD (28 h)/ZnO (12 nm)), with the details of ZnO nanowedges with nodules of silver nanoparticles grown over the nanowedges. (c) LMR absorbance spectra and (d) peak absorbance wavelength (PAW) for different concentrations of H_2O_2 solution in two operating regimes. [adapted from Ref. [61]].

C. Biological Sensing

Given the very promising and remarkable results attained, LMR-based fiber optics sensing configurations have been recently proposed in the literature for the detection of different target biomolecules, with some examples regarding molecules of diagnostic interest. The most fascinating examples from the literature account for the detection of immunoglobulin G (IgG) [10], biotin/avidin complex [62], cortisol [63], C-reactive protein (CRP) [64], and D-dimer [34].

IgG representing approximately 75% of serum antibodies in humans, is the most common type of antibody. By binding many types of pathogens, such as viruses, bacteria, and fungi, IgG protects the body from infections. The detection of IgG (≈150k g/mol) is considered as one of the gold standard to assess the performance of a biosensor [17], [65] given the standard assay protocol to be implemented and the type of biomolecule. [10] reports the generation of LMRs by the deposition of nanometer-thick metal oxide films on optical fibers and the detection of IgG in real samples of human serum. The performance has been evaluated by considering two metal oxides, i.e. ITO and SnO_2, and two types of fibers, i.e. CR-MMF and side-polished (D-shaped) fiber. Fig. 15a and b detail the two fiber configurations coated with thin films of ITO or SnO_2, together with the related experimental setups. From the comparison of the calibration curves (Fig. 15c), it is possible to observe that, given the better optical features of SnO_2 (higher *n*, real part of permittivity; lower *k*, imaginary part of permittivity) than ITO, the best performance is attained with D-shaped fibers. Therefore, SnO_2-coated (≈160 nm) D-shaped fiber LMR biosensors have been deeply characterized with repeated experiments (calibration curve shown in Fig. 15d). With a LOD of 150 pg/L (1 fM), the proposed device represents one of the best-performance biosensing platform in the literature so far.

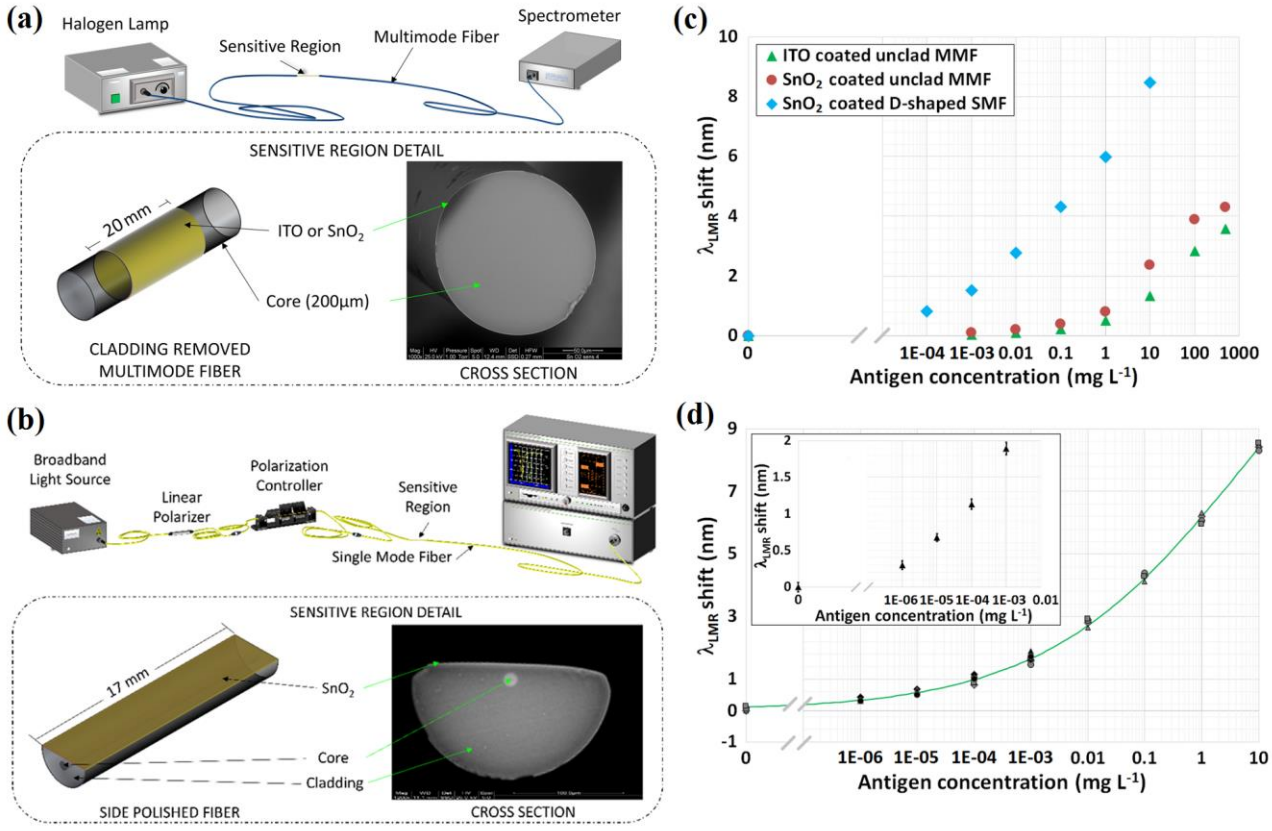

Fig. 15 (a) SEM image and sketch of the sensing device consisting of CR-MMF coated with ITO or SnO_2, together with the experimental setup. (b) SEM image and sketch of the sensing device consisting of D-shaped single-mode fiber coated with SnO_2, together with the experimental setup. (c) Comparison of the calibration curves achieved with three LMR sensors: the ITO- (green triangles) and SnO_2-coated (red circles) CR-MMF biosensors, and the SnO_2-coated D-shaped single-mode fiber biosensor (sky blue rhombuses). (d) Calibration curve of the SnO_2-coated D-shaped biosensor repeated several times and displayed together with the sigmoidal fit of the experimental points. [adapted from Ref. [10]].

Another biological complex that is routinely used to assess the performance of a biosensor consists of avitin/biotin. [62] reports a direct electrochemical functionalization of an ITO-coated LMR fiber biosensor for the detection of avidin. Electropolymerized biotin hydrazide (BH) at 10 mM is used to functionalize the fiber sensing surface by cyclic voltammetry (CV). Fig. 16a details the steps of the entire biosensing protocol: surface functionalization, receptor grafting and analyte detection. The effectiveness of the functionalization method is evaluated in terms of wavelength shift and intensity change of the LMR. All stages of the experiment are verified with optical (LMR monitoring) and electrochemical (cyclic voltammetry)

techniques simultaneously. The results achieved with CV are shown in Fig. 16b. With the dual-domain detection technique, the feasibility of the proposed label-free biosensor is demonstrated by assessing 0.01 and 0.1 mg/mL of avidin concentrations.

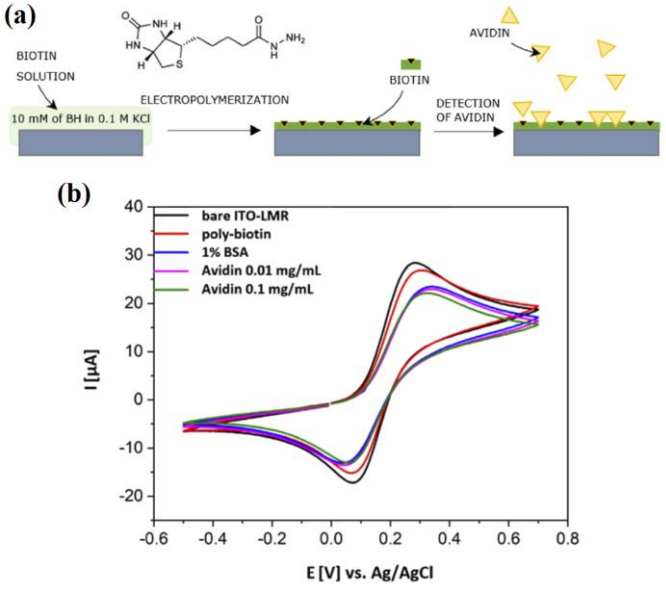

Fig. 16 (a) Schematic representation of the BH electropolymerization process and of binding of avidin to the biotinylated ITO-LMR surface. (b) CVs after each step of the assay protocol from the surface functionalization up to the avidin detection. [adapted from Ref. [62]].

Cortisol, also named as hydrocortisone, is a steroid hormone released by the chain operation of hypothalamus, pituitary and adrenal glands in response to a circumstantial trigger to human body. Cortisol plays an important role in maintaining the human homeostasis. Substantial change in its range is due to human exposure to psychological/environmental/emotional stress, and hence cortisol has been considered as the major stress hormone. Analysis of cortisol level in human body can be performed from samples of blood, sweat, hair, urine, interstitial fluids and saliva [66]. A fiber optic biosensor exploiting LMR together with molecular imprinting of nanocomposites of ZnO and polypyrrole (PPY) is presented for the detection of salivary cortisol in the concentration range of 10^{-12}–10^{-6} g/mL to cover the changing levels of salivary cortisol due to various environmental and bodily conditions [63]. Fig. 17a depicts the stages of the molecular imprinting polymer (MIP) technique, including the formation of non-imprinted layer, removal of template and interaction of analyte. Fig. 17b shows a SEM image of the optimized MIP-based ZnO/(20%ZnO/PPY) nanocomposite. Fig. 17c accounts for the spectral response in terms of absorbance changes in both the LMR wavelength and intensity for the detection of cortisol concentrations of 10^{-12}–10^{-6} g/mL. The biosensor showed the capability of detecting cortisol concentration in the range of fg/mL. Furthermore, the device possesses a high degree of stability and reusability, with a response time of around 20s.

C-reactive protein (CRP) is a homopentameric protein composed by five-polypeptide subunits (≈23k g/mol each) non-covalently associated in a ring configuration. The level of CRP in serum in healthy Caucasian people is estimated to be around 0.8 μg/mL [67]. CRP is currently considered a serum biomarker for infection or inflammation during which its concentration can rise up to 1000-fold as a consequence of some bacterial infections [67]–[69]. Very recently, it has been demonstrated that CRP levels could reflect COVID-19 disease severity and could be used as a key indicator for the monitoring of such disease [70]. Therefore, the importance of having a reliable, not so expensive, and sensitive optical technology platform for CRP quantification becomes evident. [64] reports the development of high sensitive, selective, fast response and reusable CRP aptasensors. The presented approach takes the advantages of the peculiarities of LMRs generated by ITO thin films deposited onto the flat region of D-shaped optical fibers. Fig. 18a accounts for the cross-section of the fiber optic biosensor with the details of the deposited thin films and of the implemented assay. The sensing mechanism relies on the LMR wavelength shifts originated by surface RI variations of the aptamer chain in presence of the target molecule [43]. Fig. 18b shows the calibration curve of the device when the detection of CRP concentrations of 0.0625–1 μg/mL is carried out. Additionally, the proposed device shows also high selectivity to CRP when compared to other biomolecules, such as urea or creatinine (Fig. 18c), while maintaining a low LOD (0.0625 μg/mL) and fast response time (61s).

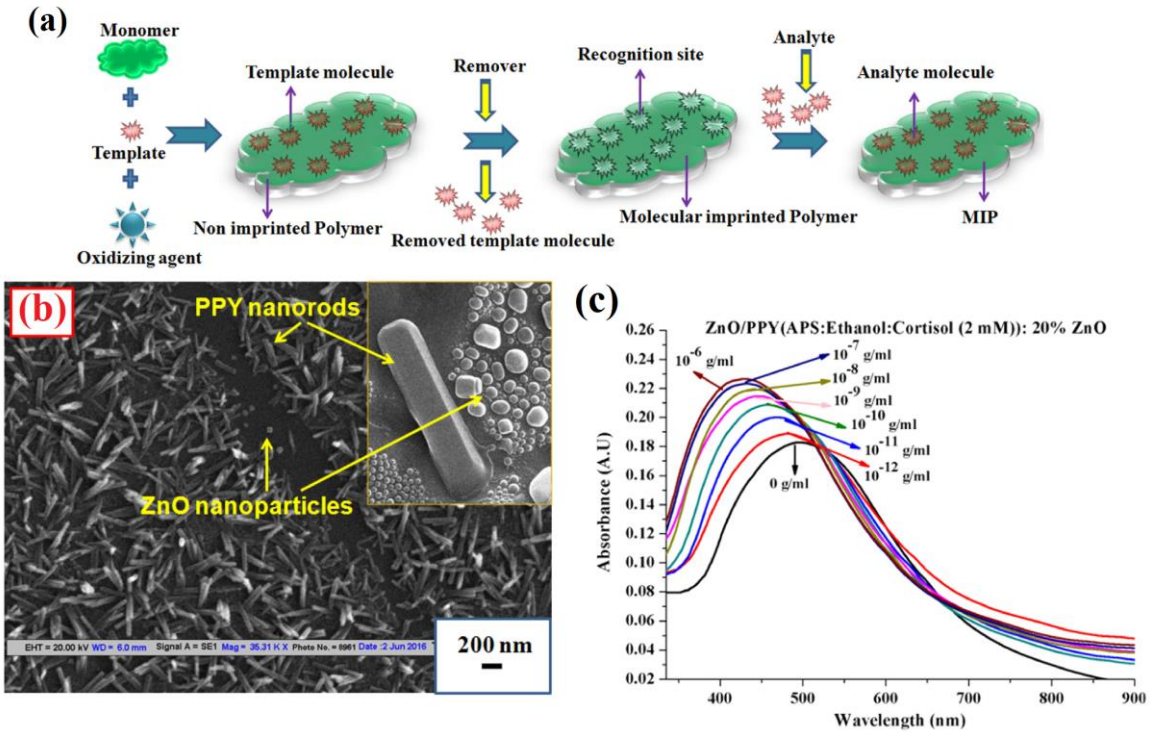

Fig. 17 (a) Schematic representation showing the stages of the molecular imprinting polymer technique including the formation of non-imprinted layer, removal of template and interaction of analyte. (b) SEM image of molecular imprinting polymers having ZnO/(20%ZnO/PPY) nanocomposite. (c) Spectral response in terms of absorbance changes in both the LMR wavelength and intensity for the detection of cortisol concentrations of 10^{-12}–10^{-6} g/mL. [adapted from Ref. [63]].

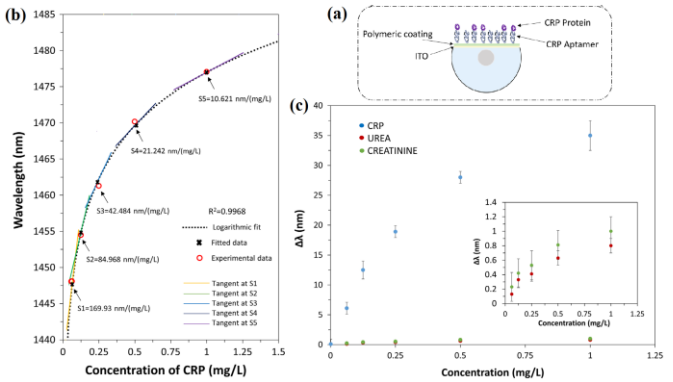

Fig. 18 (a) Cross-section of fiber optic biosensor with the details of the deposited thin films and of the implemented assay. (b) Calibration curve of the device for CRP concentrations of 0.0625–1 µg/mL., together with the surface sensitivity achieved. (c) Specificity test showing the LMR wavelength shift when the sensitive region is exposed to different concentrations of CRP (blue), urea (red) and creatinine (green). [adapted from Ref. [64]].

D-dimer antigen, the smallest product originated from cross-linked fibrin degradation, is used, above a cutoff value (0.5 µg/mL), as a biomarker for deep vein thrombosis or pulmonary embolism, collectively referred to as venous thromboembolism (VTE) [71]. About 10 million cases of VTE occur every year, thus representing the third leading vascular disease after acute myocardial infarction and stroke [72]. However, despite the importance of D-dimer monitoring by the physicians, D-dimer assays are highly variable, depending on the method of capture and on the instrumentation used. Therefore, the ability to detect in real-time the amount of D-dimer with a fast and reliable approach is a key step to anticipate the appearance of these diseases. [34] reports the results of a highly specific and sensitive biosensor for the detection of D-dimer based on LMR implemented by coating D-shaped fibers with SnO_2 thin films. The sensing principle is simply based on the measurement of LMR wavelength shift related to surface RI changes occurring when a binding interaction takes place onto the functionalized fiber portion. The device is able to detect D-dimer in human serum with a LOD of 100 ng/mL in repeated indepented experiments (n=4), a value 5-fold below the clinical cutoff value. Fig. 19a accounts for the calibration curves obtained by spiking D-dimer in human serum samples (diluted serum, blue symbols; undiluted serum, green symbols). It is clear that a LOD even lower of 10 ng/mL has been achieved in PBS, whereas a higher LOD of 320 ng/mL has been attained in undiluted serum given the highest matrix complexity. Furthermore, a technical workflow based on the separation by SDS-polyacrylamide gel electrophoresis (SDS-PAGE) and the detaction by Western-blotting (W-b) has been implemented to verify the binding of D-dimer onto the functionalized fiber surface (Fig. 19b) [34]. Fig. 19c details the experimental results of the implemented workflow. The black arrows (left) indicate the multiple bands corresponding to D-dimer protein with a specific band placed between 25 and 35 kDa (vertical black arrow). Therefore, by comparing the results achieved with mass-spectrometry-based proteomics, it is demonstrated the ability of the proposed optical technology platform to specifically (>90%) recognize D-dimer. The device potentially represents a paradigm shift in the development of a simple, high-specificity and label-free biosensing platform able to speed up diagnostic healthcare processes of VTE toward an early diagnostic and personalized treatment system.

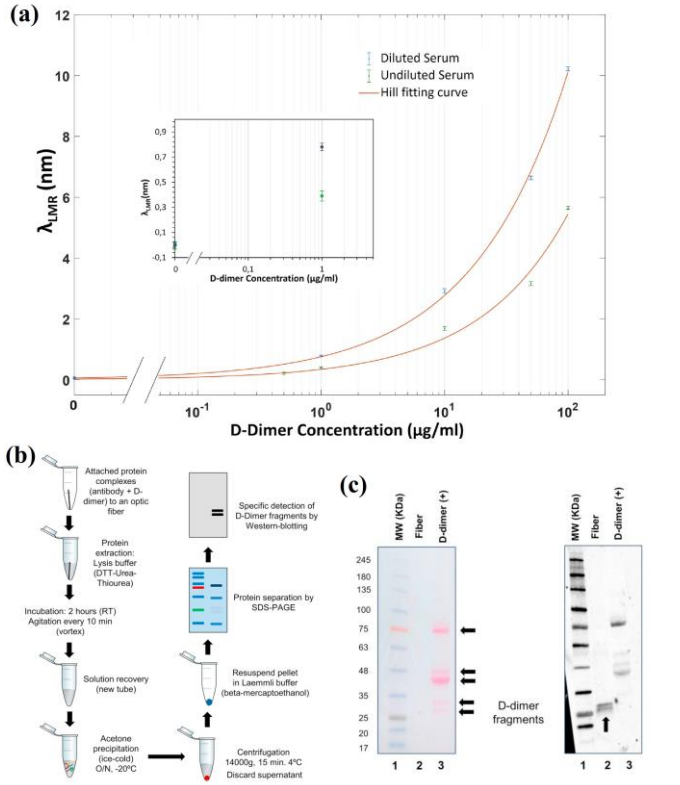

Fig. 19 (a) Calibration curves of two distinct D-shaped fiber biosensors (n=1) detecting D-dimer in human sera (diluted serum, blue symbols; undiluted serum, green symbols), together with the Hill sigmoidal fitting curves of the experimental points. The inset details the wavelength shift and error bar of the blank and first D-dimer concentrations for both cases. (b) Technical workflow used to verify the binding of D-dimer onto the functionalized biosensor surface. (c) Detection through Western-blotting of D-dimer protein detached from the functionalized fiber surface. [adapted from Ref. [34]].

IV. Conclusions and Future Perspectives

In summary, we have reported on the state-of-the-art of lossy mode resonance (LMR) devices that can be implemented on both flat surfaces (prism configuration, glass slide, coverslip, etc.) and cylindrical surfaces (glassy fiber, plastic fiber, photonic crystal fiber, etc.). Our analysis focused on optical fibers given their great potential in sensors stemming from features like: guiding properties, reduced footprint, ease of handling and the possibility to integrate them in high technological fluidic microsystems.

Two key elements are critical for LMR sensors: the geometrical configuration and the material supporting the lossy mode. Different geometries have been reviewed ranging from CMRR to tapered fibers coated with a thin film. Besides, in constrast to SPR sensor, the choice of thin film material to be deposited and that supports the LMR is vast and intese efforts are devoted to select the best material for the target applications.

Applications where LMR provided interesting results and that have been reported, can be roughly divided into three categories: physical, chemical and biological sensing. Among these, it's worth mentioning breakthrough applications that e.g. achieved detection of femtomolar (fM) concentrations with the analyte spiked in real samples of human serum, thus representing a paradigm shift towards the achievement of ultra-low detection limits with fiber-optics, with applications in early diagnostics and personalized medicine.

In the future perspectives of such a vibrant field, we envisage distinct pathways to improve the performance of LMR-based fiber-optic devices by increasing the field interaction with the analyte. Interesing routes can be summarized as follows:

- patterning of the nanometer-scale thin film deposited onto the sensitive portion of the fiber;
- implementation of a stack consisting of multi-layers of metal-oxides and composite materials;
- deposition of the nanometer-scale thin film onto the sensitive portion of the fiber with different thicknesses.

In the first case, 2D array of micro-/nano-patterns can be realized by means of e.g. focused ion beam systems (FIB/FIB-SEM) providing a light control of the lossy mode. In the second case, through an accurate modeling and controlled deposition techniques for the suitable materials an enhanced in the overlap of the lossy mode with the analyte could be realized. In last case, the deposition of the same coating material along the sensing portion of the fiber with increasing thickness can allow the excitation of multiple spectrally close LMRs. That could allow, for the very first time in fiber optic sensing, the detection of multiple parameters or biomolecules in a single sensing configuration just by tailoring the thickness of thin films, a something impossible for the state-of-the-art SPR.

LMR-based devices surely possess one of the highest RI sensitivity among fiber optic sensors. However, their resonance linewidth is at least one order of magnitude larger than other fiber optic sensors, e.g. tilted fiber gratings, and hence the device resolution and *Q*-factor should be improved in view of better performance. The above-mentioned approaches, together with specialty optical fibers or novel fiber geometries (e.g. microstructured), could lead to a further boost in LMR performances.Finally, it is also worth pointing out that the polarization-dependent sensing performance of LMR has not been exploited yet making fiber optic LMR sensor even more attractive and promising as a platform for sensor development.

References

[1] H. F. Taylor and A. Yariv, 'Guided wave optics', *Proc. IEEE*, vol. 62, no. 8, pp. 1044–1060, Aug. 1974, doi: 10.1109/PROC.1974.9569.

[2] A. R. Mickelson, *Guided Wave Optics*. Springer US, 1993.

[3] C.-L. Chen, *Foundations for guided-wave optics*. Hoboken, N.J: Wiley-Interscience, 2007.

[4] D. Kotlarek *et al.*, 'Actuated plasmonic nanohole arrays for sensing and optical spectroscopy applications', *Nanoscale*, vol. 12, no. 17, pp. 9756–9768, May 2020, doi: 10.1039/D0NR00761G.

[5] N. Maccaferri *et al.*, 'Ultrasensitive and label-free molecular-level detection enabled by light phase control in magnetoplasmonic nanoantennas', *Nat. Commun.*, vol. 6, no. 1, p. 6150, Feb. 2015, doi: 10.1038/ncomms7150.

[6] A. Sinibaldi *et al.*, 'Real-Time Study of the Adsorption and Grafting Process of Biomolecules by Means of Bloch Surface Wave Biosensors', *ACS Appl. Mater. Interfaces*,

vol. 10, no. 39, pp. 33611–33618, Oct. 2018, doi: 10.1021/acsami.8b08335.

[7] F. Chiavaioli, F. Baldini, S. Tombelli, C. Trono, and A. Giannetti, 'Biosensing with optical fiber gratings', *Nanophotonics*, vol. 6, no. 4, pp. 663–679, Jun. 2017, doi: 10.1515/nanoph-2016-0178.

[8] X. Wang and O. S. Wolfbeis, 'Fiber-Optic Chemical Sensors and Biosensors (2015–2019)', *Anal. Chem.*, vol. 92, no. 1, pp. 397–430, Jan. 2020, doi: 10.1021/acs.analchem.9b04708.

[9] C. Caucheteur, T. Guo, F. Liu, B.-O. Guan, and J. Albert, 'Ultrasensitive plasmonic sensing in air using optical fibre spectral combs', *Nat. Commun.*, vol. 7, no. 1, p. 13371, Nov. 2016, doi: 10.1038/ncomms13371.

[10] F. Chiavaioli *et al.*, 'Femtomolar Detection by Nanocoated Fiber Label-Free Biosensors', *ACS Sens.*, vol. 3, no. 5, pp. 936–943, May 2018, doi: 10.1021/acssensors.7b00918.

[11] I. D. Villar, 'Ultrahigh-sensitivity sensors based on thin-film coated long period gratings with reduced diameter, in transition mode and near the dispersion turning point', *Opt. Express*, vol. 23, no. 7, pp. 8389–8398, Apr. 2015, doi: 10.1364/OE.23.008389.

[12] M. Consales *et al.*, 'Metasurface-Enhanced Lab-on-Fiber Biosensors', *Laser Photonics Rev.*, p. 2000180, Sep. 2020, doi: 10.1002/lpor.202000180.

[13] J. Lao *et al.*, 'In situ plasmonic optical fiber detection of the state of charge of supercapacitors for renewable energy storage', *Light Sci. Appl.*, vol. 7, no. 1, p. 34, Jul. 2018, doi: 10.1038/s41377-018-0040-y.

[14] Y. Liu *et al.*, 'Plasmonic Fiber-Optic Photothermal Anemometers With Carbon Nanotube Coatings', *J. Light. Technol.*, vol. 37, no. 13, pp. 3373–3380, Jul. 2019.

[15] F. Chiavaioli, A. Giannetti, and F. Baldini, 'From Refractometry to Biosensing with Optical Fibres', in *Optical Fibre Sensors*, John Wiley & Sons, Ltd, 2020, pp. 331–366.

[16] Z. Li and F. Chiavaioli, 'In-fiber comb-like linear polarizer with leaky mode resonances', *Opt. Laser Technol.*, vol. 133, p. 106518, Jan. 2021, doi: 10.1016/j.optlastec.2020.106518.

[17] E. Gonzalez-Valencia, I. D. Villar, and P. Torres, 'Bloch waves at the surface of a single-layer coating D-shaped photonic crystal fiber', *Opt. Lett.*, vol. 45, no. 9, pp. 2547–2550, May 2020, doi: 10.1364/OL.391508.

[18] B. Špačková, N. S. Lynn, J. Slabý, H. Šípová, and J. Homola, 'A Route to Superior Performance of a Nanoplasmonic Biosensor: Consideration of Both Photonic and Mass Transport Aspects', *ACS Photonics*, vol. 5, no. 3, pp. 1019–1025, Mar. 2018, doi: 10.1021/acsphotonics.7b01319.

[19] M. Marciniak, J. Grzegorzewski, and M. Szustakowski, 'Analysis of lossy mode cut-off conditions in planar waveguides with semiconductor guiding layer', *IEE Proc. J - Optoelectron.*, vol. 140, no. 4, pp. 247–252, Aug. 1993, doi: 10.1049/ip-j.1993.0040.

[20] F. Yang and J. R. Sambles, 'Determination of the optical permittivity and thickness of absorbing films using long range modes', *J. Mod. Opt.*, vol. 44, no. 6, pp. 1155–1163, Jun. 1997, doi: 10.1080/09500349708230726.

[21] A. B. Socorro-Leránoz, D. Santano, I. Del Villar, and I. R. Matias, 'Trends in the design of wavelength-based optical fibre biosensors (2008–2018)', *Biosens. Bioelectron. X*, vol. 1, p. 100015, Jun. 2019, doi: 10.1016/j.biosx.2019.100015.

[22] I. Del Villar *et al.*, 'Optical sensors based on lossy-mode resonances', *Sens. Actuators B Chem.*, vol. 240, pp. 174–185, Mar. 2017, doi: 10.1016/j.snb.2016.08.126.

[23] I. D. Villar, V. Torres, and M. Beruete, 'Experimental demonstration of lossy mode and surface plasmon resonance generation with Kretschmann configuration', *Opt. Lett.*, vol. 40, no. 20, pp. 4739–4742, Oct. 2015, doi: 10.1364/OL.40.004739.

[24] M. Born and E. Wolf, *Principles of Optics: Electromagnetic Theory of Propagation, Interference and Diffraction of Light*, 7th ed. Cambridge: Cambridge University Press, 1999.

[25] N. Paliwal and J. John, 'Lossy Mode Resonance (LMR) Based Fiber Optic Sensors: A Review', *IEEE Sens. J.*, vol. 15, no. 10, pp. 5361–5371, Oct. 2015, doi: 10.1109/JSEN.2015.2448123.

[26] I. D. Villar, C. R. Zamarreno, M. Hernaez, F. J. Arregui, and I. R. Matias, 'Lossy Mode Resonance Generation With Indium-Tin-Oxide-Coated Optical Fibers for Sensing Applications', *J. Light. Technol.*, vol. 28, no. 1, pp. 111–117, Jan. 2010, doi: 10.1109/JLT.2009.2036580.

[27] C. R. Zamarreño, M. Hernáez, I. Del Villar, I. R. Matías, and F. J. Arregui, 'Optical fiber pH sensor based on lossy-mode resonances by means of thin polymeric coatings', *Sens. Actuators B Chem.*, vol. 155, no. 1, pp. 290–297, Jul. 2011, doi: 10.1016/j.snb.2010.12.037.

[28] A. K. Sharma and B. D. Gupta, 'On the sensitivity and signal to noise ratio of a step-index fiber optic surface plasmon resonance sensor with bimetallic layers', *Opt. Commun.*, vol. 245, no. 1, pp. 159–169, Jan. 2005, doi: 10.1016/j.optcom.2004.10.013.

[29] A. Shalabney and I. Abdulhalim, 'Electromagnetic fields distribution in multilayer thin film structures and the origin of sensitivity enhancement in surface plasmon resonance sensors', *Sens. Actuators Phys.*, vol. 159, no. 1, pp. 24–32, Apr. 2010, doi: 10.1016/j.sna.2010.02.005.

[30] X. (王雪州) Wang, Q. (王琦) Wang, Z. (宋志伟) Song, and K. (齐康如) Qi, 'Simulation of a microstructure fiber pressure sensor based on lossy mode resonance', *AIP Adv.*, vol. 9, no. 9, p. 095005, Sep. 2019, doi: 10.1063/1.5112090.

[31] L. Chen, *Microwave electronics: measurement and materials characterization*. Chichester: Wiley, 2005.

[32] K. Kosiel, M. Koba, M. Masiewicz, and M. Śmietana, 'Tailoring properties of lossy-mode resonance optical fiber sensors with atomic layer deposition technique', *Opt. Laser Technol.*, vol. 102, pp. 213–221, Jun. 2018, doi: 10.1016/j.optlastec.2018.01.002.

[33] A. Ozcariz, C. Ruiz-Zamarreño, and F. J. Arregui, 'A Comprehensive Review: Materials for the Fabrication of Optical Fiber Refractometers Based on Lossy Mode

Resonance', *Sensors*, vol. 20, no. 7, Apr. 2020, doi: 10.3390/s20071972.

[34] P. Zubiate *et al.*, 'Fiber-based early diagnosis of venous thromboembolic disease by label-free D-dimer detection', *Biosens. Bioelectron. X*, vol. 2, p. 100026, Oct. 2019, doi: 10.1016/j.biosx.2019.100026.

[35] I. D. Villar *et al.*, 'Design rules for lossy mode resonance based sensors', *Appl. Opt.*, vol. 51, no. 19, pp. 4298–4307, Jul. 2012, doi: 10.1364/AO.51.004298.

[36] A. Ozcariz, C. R. Zamarreño, P. Zubiate, and F. J. Arregui, 'Is there a frontier in sensitivity with Lossy mode resonance (LMR) based refractometers?', *Sci. Rep.*, vol. 7, no. 1, p. 10280, Aug. 2017, doi: 10.1038/s41598-017-11145-9.

[37] P.-C. P, Á.-T. Ri, G.-M. M, and D.-S. M, 'Lossy Mode Resonance Generation on Sputtered Aluminum-Doped Zinc Oxide Thin Films Deposited on Multimode Optical Fiber Structures for Sensing Applications in the 1.55 μm Wavelength Range.', *Sensors*, vol. 19, no. 19, Sep. 2019, doi: 10.3390/s19194189.

[38] P. Sánchez, C. R. Zamarreño, F. J. Arregui, and I. R. Matías, 'LMR-Based Optical Fiber Refractometers for Oil Degradation Sensing Applications in Synthetic Lubricant Oils', *J. Light. Technol.*, vol. 34, no. 19, pp. 4537–4542, Oct. 2016.

[39] P. Sanchez, C. R. Zamarreno, M. Hernaez, I. D. Villar, I. R. Matias, and F. J. Arregui, 'Considerations for Lossy-Mode Resonance-Based Optical Fiber Sensor', *IEEE Sens. J.*, vol. 13, no. 4, pp. 1167–1171, Apr. 2013, doi: 10.1109/JSEN.2012.2227717.

[40] P. J. Rivero, A. Urrutia, J. Goicoechea, and F. J. Arregui, 'Optical fiber humidity sensors based on Localized Surface Plasmon Resonance (LSPR) and Lossy-mode resonance (LMR) in overlays loaded with silver nanoparticles', *Sens. Actuators B Chem.*, 2012, Accessed: Nov. 09, 2020. [Online]. Available: https://agris.fao.org/agris-search/search.do?recordID=US201500115972.

[41] J. Ascorbe, J. M. Corres, F. J. Arregui, and I. R. Matías, 'Optical Fiber Current Transducer Using Lossy Mode Resonances for High Voltage Networks', *J. Light. Technol.*, vol. 33, no. 12, pp. 2504–2510, Jun. 2015.

[42] J. M. Corres, J. Ascorbe, F. J. Arregui, and I. R. Matias, 'Tunable electro-optic wavelength filter based on lossy-guided mode resonances', *Opt. Express*, vol. 21, no. 25, pp. 31668–31677, Dec. 2013, doi: 10.1364/OE.21.031668.

[43] F. Chiavaioli, C. A. J. Gouveia, P. A. S. Jorge, and F. Baldini, 'Towards a Uniform Metrological Assessment of Grating-Based Optical Fiber Sensors: From Refractometers to Biosensors', *Biosensors*, vol. 7, no. 2, Jun. 2017, doi: 10.3390/bios7020023.

[44] A. Ozcariz, D. A. Piña-Azamar, C. R. Zamarreño, R. Dominguez, and F. J. Arregui, 'Aluminum doped zinc oxide (AZO) coated optical fiber LMR refractometers—An experimental demonstration', *Sens. Actuators B Chem.*, vol. 281, pp. 698–704, Feb. 2019, doi: 10.1016/j.snb.2018.10.158.

[45] A. Andreev *et al.*, 'A refractometric sensor using index-sensitive mode resonance between single-mode fiber and thin film amorphous silicon waveguide', *Sens. Actuators B Chem.*, vol. 106, no. 1, pp. 484–488, Apr. 2005, doi: 10.1016/j.snb.2004.09.002.

[46] A. T. Andreev, B. S. Zafirova, E. I. Karakoleva, A. O. Dikovska, and P. A. Atanasov, 'Highly sensitive refractometers based on a side-polished single-mode fibre coupled with a metal oxide thin-film planar waveguide', *J. Opt. Pure Appl. Opt.*, vol. 10, p. 035303, Mar. 2008, doi: 10.1088/1464-4258/10/3/035303.

[47] C. R. Zamarreno *et al.*, 'Sensing Properties of Indium Oxide Coated Optical Fiber Devices Based on Lossy Mode Resonances', *IEEE Sens. J.*, vol. 12, no. 1, pp. 151–155, Jan. 2012, doi: 10.1109/JSEN.2011.2142181.

[48] W.-M. Zhao, Q. Wang, X.-Z. Wang, X. Li, J.-Y. Jing, and H.-Z. Sun, 'Theoretical and experimental research of lossy mode resonance-based high-sensitivity optical fiber refractive index sensors', *JOSA B*, vol. 36, no. 8, pp. 2069–2078, Aug. 2019, doi: 10.1364/JOSAB.36.002069.

[49] C.-L. Tien, H.-Y. Lin, and S.-H. Su, 'High Sensitivity Refractive Index Sensor by D-Shaped Fibers and Titanium Dioxide Nanofilm', *Advances in Condensed Matter Physics*, Feb. 05, 2018. https://www.hindawi.com/journals/acmp/2018/2303740/ (accessed Nov. 09, 2020).

[50] A. Ozcariz, M. Dominik, M. Smietana, C. R. Zamarreño, I. Del Villar, and F. J. Arregui, 'Lossy mode resonance optical sensors based on indium-gallium-zinc oxide thin film', *Sens. Actuators Phys.*, vol. 290, pp. 20–27, May 2019, doi: 10.1016/j.sna.2019.03.010.

[51] P. Zubiate, C. R. Zamarreño, I. D. Villar, I. R. Matias, and F. J. Arregui, 'High sensitive refractometers based on lossy mode resonances (LMRs) supported by ITO coated D-shaped optical fibers', *Opt. Express*, vol. 23, no. 6, pp. 8045–8050, Mar. 2015, doi: 10.1364/OE.23.008045.

[52] Q. Wang, X. Li, W.-M. Zhao, and S. Jin, 'Lossy mode resonance-based fiber optic sensor using layer-by-layer SnO2 thin film and SnO2 nanoparticles', *Appl. Surf. Sci.*, vol. 492, pp. 374–381, Oct. 2019, doi: 10.1016/j.apsusc.2019.06.168.

[53] M. Hernaez, A. G. Mayes, and S. Melendi-Espina, 'Graphene Oxide in Lossy Mode Resonance-Based Optical Fiber Sensors for Ethanol Detection', *Sensors*, vol. 18, no. 1, p. 58, Jan. 2018, doi: 10.3390/s18010058.

[54] A. B. Socorro, I. D. Villar, J. M. Corres, F. J. Arregui, and I. R. Matias, 'Spectral width reduction in lossy mode resonance-based sensors by means of tapered optical fibre structures', *Sens. Actuators B Chem.*, vol. 200, pp. 53–60.

[55] Q. Wang, W.-M. Zhao, J.-Y. Jing, and X.-Z. Wang, 'Lossy mode resonance generated by titanium dioxide nanoarray: a comprehensive theoretical research', *J. Opt.*, vol. 22, no. 3, p. 035004, Feb. 2020, doi: 10.1088/2040-8986/ab68ed.

[56] R. Su, G. Zhong, Q. Fu, L. Zhang, H. Fong, and L. Zhu, 'Polarity-induced ferroelectric crystalline phase in electrospun fibers of poly(vinylidene fluoride)/polyacrylonitrile blends', *J. Mater. Res.*, vol. 27, no. 10, pp. 1389–1398, May 2012, doi: 10.1557/jmr.2012.56.

[57] S. K. Mishra, S. P. Usha, and B. D. Gupta, 'A lossy mode resonance-based fiber optic hydrogen gas sensor for room temperature using coatings of ITO thin film and nanoparticles', *Meas. Sci. Technol.*, vol. 27, no. 4, p. 045103, Feb. 2016, doi: 10.1088/0957-0233/27/4/045103.

[58] S. P. Usha, S. K. Mishra, and B. D. Gupta, 'Fiber optic hydrogen sulfide gas sensors utilizing ZnO thin film/ZnO nanoparticles: A comparison of surface plasmon resonance and lossy mode resonance', *Sens. Actuators B Chem.*, vol. 218, pp. 196–204, Oct. 2015, doi: 10.1016/j.snb.2015.04.108.

[59] C. Elosua *et al.*, 'Volatile organic compounds optical fiber sensor based on lossy mode resonances', *Sens. Actuators B Chem.*, 2012, Accessed: Nov. 09, 2020. [Online]. Available: https://agris.fao.org/agris-search/search.do?recordID=US201500116020.

[60] D. Tiwari, K. Mullaney, S. Korposh, S. W. James, S.-W. Lee, and R. P. Tatam, 'An ammonia sensor based on Lossy Mode Resonances on a tapered optical fibre coated with porphyrin-incorporated titanium dioxide', *Sens. Actuators B Chem.*, vol. 242, pp. 645–652, Apr. 2017, doi: 10.1016/j.snb.2016.11.092.

[61] S. P. Usha, A. M. Shrivastav, and B. D. Gupta, 'Silver nanoparticle noduled ZnO nanowedge fetched novel FO-LMR based H2O2 biosensor: A twin regime sensor for in-vivo applications and H2O2 generation analysis from polyphenolic daily devouring beverages', *Sens. Actuators B Chem.*, vol. 241, pp. 129–145, Mar. 2017, doi: 10.1016/j.snb.2016.10.067.

[62] M. Janik *et al.*, 'Electrochemically directed biofunctionalization of a lossy-mode resonance optical fiber sensor', *Opt. Express*, vol. 28, no. 11, pp. 15934–15942, May 2020, doi: 10.1364/OE.390780.

[63] S. P. Usha, A. M. Shrivastav, and B. D. Gupta, 'A contemporary approach for design and characterization of fiber-optic-cortisol sensor tailoring LMR and ZnO/PPY molecularly imprinted film', *Biosens. Bioelectron.*, vol. 87, pp. 178–186, Jan. 2017, doi: 10.1016/j.bios.2016.08.040.

[64] P. Zubiate, C. R. Zamarreño, P. Sánchez, I. R. Matias, and F. J. Arregui, 'High sensitive and selective C-reactive protein detection by means of lossy mode resonance based optical fiber devices', *Biosens. Bioelectron.*, vol. 93, pp. 176–181, Jul. 2017, doi: 10.1016/j.bios.2016.09.020.

[65] F. Baldini, M. Brenci, F. Chiavaioli, A. Giannetti, and C. Trono, 'Optical fibre gratings as tools for chemical and biochemical sensing', *Anal. Bioanal. Chem.*, vol. 402, no. 1, pp. 109–116, Jan. 2012, doi: 10.1007/s00216-011-5492-3.

[66] C. Tlili, N. V. Myung, V. Shetty, and A. Mulchandani, 'Label-free, chemiresistor immunosensor for stress biomarker cortisol in saliva', *Biosens. Bioelectron.*, vol. 26, no. 11, pp. 4382–4386, Jul. 2011, doi: 10.1016/j.bios.2011.04.045.

[67] N. R. Sproston and J. J. Ashworth, 'Role of C-Reactive Protein at Sites of Inflammation and Infection', *Front. Immunol.*, vol. 9, p. 754, 2018, doi: 10.3389/fimmu.2018.00754.

[68] F. Esposito *et al.*, 'Long period grating in double cladding fiber coated with graphene oxide as high-performance optical platform for biosensing', *Biosens. Bioelectron.*, vol. 172, p. 112747, Jan. 2021, doi: 10.1016/j.bios.2020.112747.

[69] A. Aray *et al.*, 'SPR-based plastic optical fibre biosensor for the detection of C-reactive protein in serum', *J. Biophotonics*, vol. 9, no. 10, pp. 1077–1084, 2016, doi: 10.1002/jbio.201500315.

[70] L. Wang, 'C-reactive protein levels in the early stage of COVID-19', *Med. Mal. Infect.*, vol. 50, no. 4, pp. 332–334, Jun. 2020, doi: 10.1016/j.medmal.2020.03.007.

[71] M. Di Nisio, N. van Es, and H. R. Büller, 'Deep vein thrombosis and pulmonary embolism', *Lancet Lond. Engl.*, vol. 388, no. 10063, pp. 3060–3073, 17 2016, doi: 10.1016/S0140-6736(16)30514-1.

[72] L.-A. Linkins and S. Takach Lapner, 'Review of D-dimer testing: Good, Bad, and Ugly', *Int. J. Lab. Hematol.*, vol. 39 Suppl 1, pp. 98–103, May 2017, doi: 10.1111/ijlh.12665.

Biography of Authors

Francesco Chiavaioli received the M.Sc. degree (*summa cum laude*) in Telecommunications Engineering and the Ph.D. degree in Information Engineering from the University of Siena, Italy, in 2008 and 2012, respectively. He started working as fixed-term researcher at the Institute of Applied Physics "Nello Carrara", National Research Council (CNR-IFAC), Italy, in the design and characterization of novel optical fiber sensors, especially based on fiber Bragg gratings and long period gratings, for the detection of physical, chemical, and biological parameters. In 2015–2016, he spent seven months as a Visiting Scientist at the Institute of Photonic Sciences (ICFO), Barcelona, Spain, during which he worked with thin films, graphene-based nanocavities and optical modulators. From December 2018, he works as permanent researcher at CNR-IFAC and his research activity is focusing on guided-wave optics, fiber-optics, sensing and biosensing optical platforms, biophotonics, resonance-based devices, whispering gallery mode resonators, probes for the measurement of bile and pH, and novel in-fiber photonic nanostructures. He is actively working in several European, Bilateral and National projects. He is part of the Editorial board of MDPI Optics and of the Programme Committee of SPIE Photonics Europe conference (Optical Sensing and Detection session). He is author of more than 60 publications on the subjects in ISI Journals and in Conference Proceedings. He was awarded by IEEE, OSA and IOP as Outstanding Reviewer recipient in 2018, 2019 and 2020, respectively. He is Member of IEEE, OSA, SPIE, EOS, and SIOF.

Davide Luca Janner received his Ph.D. in Physics from Politecnico di Milano in 2006 and his M.Sc. degree in Physics from Università degli Studi di Milano, Milan (Italy), in 2002. During his Ph.D. he studied light propagation and its localization effects in periodic media both from a theoretical and experimental point of view. From 2006 to the end of 2015 he joined ICFO-The Institute of Photonic Sciences as a junior post-doctoral researcher working on acousto-optic and electro-optic devices for telecommunication and sensing, specializing on techniques of micro- and nano-fabrication. Since December 2015 is Associate Professor in Materials Science and his research topics are currently focused on bioresorbable and active glass materials for photonics applications, photonic sensors and micro-/nano-structured multifunctional materials.